Topological Higgs amplitude modes in strongly interacting superfluids

Junsen Wang,[1,2] Youjin Deng,[1,2,3] and Wei Zheng[1,2,*]

[1]*Department of Modern Physics, Hefei National Laboratory for Physical Sciences at Microscale, University of Science and Technology of China, Hefei, Anhui 230026, China*

[2]*CAS Center for Excellence and Synergetic Innovation Center in Quantum Information and Quantum Physics, University of Science and Technology of China, Hefei, Anhui 230026, China*

[3]*MinJiang Collaborative Center for Theoretical Physics, College of Physics and Electronic Information Engineering, Minjiang University, Fuzhou 350108, China*

(Received 26 July 2021; accepted 18 October 2021; published 29 October 2021)

By studying the two-dimensional Su-Schrieffer-Heeger-Bose-Hubbard model, we show the existence of topological Higgs amplitude modes in the strongly interacting superfluid phase. Using the slave boson approach, we find that, in the large filling limit, the Higgs excitations and the Goldstone excitations above the ground state are well decoupled, and both of them exhibit nontrivial topology inherited from the underlying noninteracting bands. At finite fillings, they become coupled at high energies; nevertheless, the topology of these modes remains unchanged. Based on an effective action analysis, we further provide a universal physical picture for both their topological and phase-amplitude character at both infinite and finite fillings in a unified way. The discovery of topological Higgs amplitude modes in this paper opens the path to investigations in various systems, such as superconductors and quantum magnets.

DOI: 10.1103/PhysRevA.104.043328

I. INTRODUCTION

Topological matter has been playing a central role in modern condensed-matter physics since its discovery in integer quantum Hall effects [1] about 40 yr ago. In those early days, topological properties manifest themselves via quantized bulk observables, which are directly linked to topological invariants [2]. Later, it was found that nontrivial bulk topology can introduce robust edge modes. An important insight from Haldane and Raghu [3] is that this central topological phenomenon is essentially a *wave effect* not necessarily tied to fermions. As a result, there is a recent trend to study various systems with no fermionic analog, e.g., topological photonics [4,5], topological phonons [6,7], topological magnons [8–11], topological mechanics and acoustics [12–14], even topological atmospheric and ocean waves [15]. In particular, cold atomic systems as quantum simulators [16,17], provide a unique possibility to study topological Bose superfluids, whose Bogoliubov excitations in the weak-coupling limit also have a topological band structure [18–29]. These topological quasiparticles as bosonic in nature are similar to topological phonons and magnons, which possess robust edge modes dictated by the bulk-boundary correspondence and are detectable by spectroscopy measurements. So far, studies have been carried out only for the topology of the Nambu-Goldstone mode [30,31] in the weak-coupling region, which is gapless at low energies.

One notes that the spontaneous breaking of a continuous symmetry leads to two types of collective excitations: the gapless Nambu-Goldstone mode and the gapped Higgs mode [32]. In the standard model of particle physics, the famous Higgs boson [33], being elusive for decades, was finally discovered recently [34,35]. As its close cousin in condensed-matter physics, the Higgs amplitude mode [36] also attracts much attention and has been experimentally found in superconductors [37–39], charge-density waves [40], quantum magnets [41,42], and the superfluid ^{3}He -B phase [43,44]. In the strongly interacting superfluid phase of the Bose-Hubbard model (BHM) realized in cold-atomic systems [45,46], this mode has also been discussed extensively [47–51], and its observation has been reported recently using Bragg spectroscopy [52] and using lattice modulation [53].

Can the Higgs amplitude modes also be topologically nontrivial? Here we give an affirmative answer to this question by studying a simple variant of the two-dimensional (2D) BHM in the strong-coupling limit, which can be easily implemented experimentally in cold-atom platforms. We find that, in the large filling limit, the Higgs mode and the Goldstone mode are well decoupled, and both of them exhibit nontrivial topology inherited from the background noninteracting bands. At finite fillings, they become coupled at high energies; nevertheless, the topology of these modes is unchanged. Based on an effective action analysis, we further provide a universal physical picture for the topology of Higgs and Goldstone modes, which could also be possibly applicable to other symmetry-breaking systems, such as superconductors and quantum magnets.

II. MODEL

As a concrete and minimal example to host topological Higgs amplitude modes, we consider the 2D Su-Schrieffer-Heeger-Bose-Hubbard Model (SSH-BHM), described by the Hamiltonian,

$$\hat{H} = \hat{H}^{\mathrm{hop}} + \frac{1}{2}U\sum_i \hat{n}_i(\hat{n}_i - 1) - \mu\sum_i \hat{n}_i, \qquad (1)$$

*zw8796@ustc.edu.cn

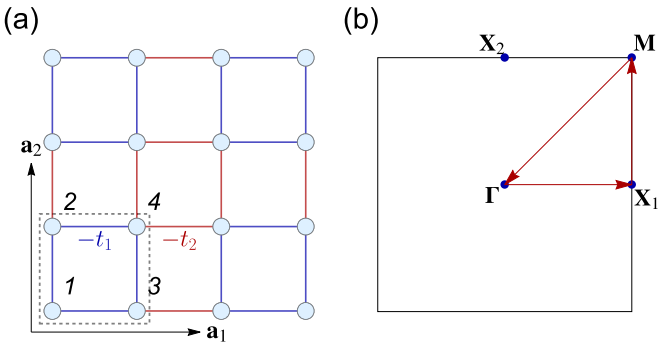

FIG. 1. (a) Two-dimensional SSH-BHM on a square lattice. A unit cell is enclosed by a gray dashed square with four sublattices labeled by an index $\eta = 1, \ldots, 4$. The intracell (intercell) hopping strength is $-t_1$ ($-t_2$), shown in the blue (red) color. Black arrows are two primitive lattice vectors $\mathbf{a}_{1,2}$. We set $|\mathbf{a}_1| = |\mathbf{a}_2| = 1$ as the length unit. (b) The first Brillouin zone (BZ) of the model. Four inversion symmetric points are shown explicitly. The red vectors denote the high-symmetric path used in Figs. 3(a) and 3(d).

where $\hat{H}^{\text{hop}} = -\sum_{ij} t_{ij}\hat{a}_i^\dagger \hat{a}_j = \sum_{\mathbf{k}} H_{\mathbf{k}}^{\text{hop}} \hat{a}_{\mathbf{k}}^\dagger \hat{a}_{\mathbf{k}}$ is the kinetic term with the staggered hopping amplitudes along both directions as depicted in Fig. 1. This hopping Hamiltonian is the 2D generalization of the SSH model [54] introduced in Refs. [55–57], whose band topology is protected by the inversion symmetry $\mathcal{I} H_{-\mathbf{k}}^{\text{hop}} \mathcal{I}^{-1} = H_{\mathbf{k}}^{\text{hop}}$ where in the basis specified by Fig. 1, the inversion operator reads $\mathcal{I} = \sigma_1 \otimes \sigma_1$, and σ_1 is the standard Pauli matrix. The corresponding topological invariant is the vectorized Zak phase, also equal to the macroscopic polarization vector [58]. Due to inversion symmetry, each component of the polarization vector is quantized to a $\mathbb{Z}_2$ index [59]. With the additional C_4 symmetry, the polarization center either coincides with the original square lattice (for $t_1 > t_2$, the trivial phase) or coincides with its dual lattice (for $t_1 < t_2$, the topological phase). Note that this topological index can be inferred from the eigenvalues of $\mathcal{I}$ at inversion symmetric momenta [59,60].

This model Hamiltonian can be realized in experiments by loading spinless bosons in a square optical lattice with the addition of a period-2 superlattice. In the following we will focus on the case where t_1/t_2 is not far from unity. In this region, there is a quantum phase transition between Mott-insulating (MI) and superfluid (SF) phase driven by t/U, where $t = (t_1 + t_2)/2$ with the superfluid order parameter simply given by $\varphi = \langle a_i \rangle$ [45].

III. LARGE FILLING LIMIT

We utilize the slave boson approach [47,48,61–66] to study the excitation spectrums in the SF phase. The basic idea of the slave boson method is to enlarge the local Hilbert space by introducing bosonic operators $\hat{b}_{i,n_i}^\dagger$ that create the local Fock state as $\hat{b}_{i,n_i}^\dagger|\text{vac}\rangle = (\hat{a}_i^\dagger)^{n_i}/\sqrt{n_i!}|0\rangle$, where $|0\rangle$ is the physical vacuum state and $|\text{vac}\rangle$ is the vacuum state of the slave bosons. The original bosonic operators $\hat{a}_i^\dagger$ then can be expressed in terms of the slave boson operators $\hat{a}_i^\dagger = \sum_{n_i} \sqrt{n_i+1}\hat{b}_{i,n_i+1}^\dagger \hat{b}_{i,n_i}$. To keep the canonical commutation relations of physical bosonic operators, one has to impose a local constraint $\sum_{n_i} \hat{b}_{i,n_i}^\dagger \hat{b}_{i,n_i} = 1$.

In the vicinity of the SF-MI transition at the qth lobe, where q is a non-negative integer, the particle number fluctuation is highly suppressed such that we can truncate the local Hilbert space by keeping only three relevant states $|q\rangle_i$ and $|q \pm 1\rangle_i$. Then we consider the large filling limit $q \gg 1$ such that the particle and hole excitations have the same Bose enhancement factors $\sqrt{q+1} \simeq \sqrt{q}$. Therefore, the physical bosons now are given by $\hat{a}_i^\dagger \simeq \sqrt{q}(\hat{b}_{i,q+1}^\dagger \hat{b}_{i,q} + \hat{b}_{i,q}^\dagger \hat{b}_{i,q-1})$, and the local constraint of the slave bosons becomes $\sum_{\ell=-1}^{1} \hat{b}_{i,q+\ell}^\dagger \hat{b}_{i,q+\ell} = 1$. The slave boson approach starts from the local mean-field Hamiltonian $\hat{H}_i^{\text{MF}} = -zt\varphi(\hat{a}_i + \hat{a}_i^\dagger) + \frac{1}{2}U\hat{n}_i(\hat{n}_i - 1) - \mu\hat{n}_i$. Using slave boson operators, the mean-field Hamiltonian can be recast as

$$\hat{H}_i^{\text{MF}} = [\hat{b}_{i,q+1}^\dagger \quad \hat{b}_{i,q}^\dagger \quad \hat{b}_{i,q-1}^\dagger] \begin{bmatrix} \frac{U}{2} & \frac{zt\varphi}{\sqrt{q}} & 0 \\ & 0 & \frac{zt\varphi}{\sqrt{q}} \\ \text{H.c.} & & \frac{U}{2} \end{bmatrix} \begin{bmatrix} \hat{b}_{i,q+1} \\ \hat{b}_{i,q} \\ \hat{b}_{i,q-1} \end{bmatrix}, \tag{2}$$

where $\mu = q - 1/2$ is used, corresponding to the so-called particle-hole (PH) symmetric line (see Appendix A for details), and a constant term is omitted. Given a φ, Eq. (2) can be diagonalized by a rotation,

$$\begin{bmatrix} \hat{\beta}_{i,G} \\ \hat{\beta}_{i,A} \\ \hat{\beta}_{i,P} \end{bmatrix} = \frac{1}{\sqrt{2}} \begin{bmatrix} \sin\frac{\theta}{2} & \sqrt{2}\cos\frac{\theta}{2} & \sin\frac{\theta}{2} \\ \cos\frac{\theta}{2} & -\sqrt{2}\sin\frac{\theta}{2} & \cos\frac{\theta}{2} \\ 1 & 0 & -1 \end{bmatrix} \begin{bmatrix} \hat{b}_{i,q-1} \\ \hat{b}_{i,q} \\ \hat{b}_{i,q+1} \end{bmatrix}, \tag{3}$$

where $\theta = \arccos(U/16\tilde{t})$ and $\tilde{t} = qt$. The ground state obtained, in turn, determines the parameter φ; one, therefore, can self-consistently solve this mean-field Hamiltonian [67]. Note the local constraint is preserved under this unitary rotation. One can straightforwardly rewrite the original Hamiltonian Eq. (1) using these rotated slave bosons. In this representation, the on-site interaction term becomes quadratic, whereas the hopping term becomes quartic (see Appendix B for the explicit expression). Note that the rotated slave boson $\hat{\beta}_{i,G}$ generates the mean-field ground-state $|G\rangle = \prod_i \hat{\beta}_{i,G}^\dagger|\text{vac}\rangle$; whereas $\hat{\beta}_{i,P}$ and $\hat{\beta}_{i,A}$ build up the local excitations. We, therefore, condense $\hat{\beta}_{i,G}$, namely, set $\hat{\beta}_{i,G} \simeq \hat{\beta}_{i,G}^\dagger \simeq 1$ and treat others as small fluctuations. Then one can expand Eq. (1) up to quadratic order in the rotated slave bosons $\hat{H} \simeq \hat{H}^{(2)}$ where

$$\hat{H}^{(2)} = \frac{1}{2}\sum_{\mathbf{k}\in\text{BZ}} [\hat{\Psi}_{\mathbf{k},A}^\dagger \quad \hat{\Psi}_{\mathbf{k},P}^\dagger] H_{\mathbf{k}}^{(2)} \begin{bmatrix} \hat{\Psi}_{\mathbf{k},A} \\ \hat{\Psi}_{\mathbf{k},P} \end{bmatrix}, \tag{4}$$

where a constant term is omitted and the first-order term $\hat{H}^{(1)}$ vanishes by construction. Here the Nambu spinor is defined by $\hat{\Psi}_{\mathbf{k},\alpha} = (\hat{\beta}_{\mathbf{k},1,\alpha}, \ldots, \hat{\beta}_{\mathbf{k},4,\alpha}, \hat{\beta}_{-\mathbf{k},1,\alpha}^\dagger, \ldots, \hat{\beta}_{-\mathbf{k},4,\alpha}^\dagger)$, $\alpha = A, P$, and $\hat{\beta}_{\mathbf{k},\sigma,\alpha} = \frac{1}{\sqrt{N}}\sum_l e^{i\mathbf{k}\cdot\mathbf{r}_l}\hat{\beta}_{l,\eta,\alpha}$ with N being the total unit-cell number. In the large filling limit, it turns out that $H_{\mathbf{k}}^{(2)} = H_{\mathbf{k},A}^{\text{BdG}} \oplus H_{\mathbf{k},P}^{\text{BdG}}$, where BdG represents Bogoliubov–de Gennes, i.e., two local excitation modes are decoupled, which enables us to write $\hat{H}^{(2)} = \frac{1}{2}\sum_{\mathbf{k},\alpha=A,P} \hat{\Psi}_{\mathbf{k},\alpha}^\dagger H_{\mathbf{k},\alpha}^{\text{BdG}} \hat{\Psi}_{\mathbf{k},\alpha}$. Here

TABLE I. Parameters used in Eq. (5) for amplitude modes ($\alpha = A$) and phase modes ($\alpha = P$).

	ξ_α	κ_α	ζ_α
$\alpha = A$	$2z\tilde{t}\,\sin^2\theta + \frac{1}{2}U\,\cos\theta$	$\cos^2\theta$	1
$\alpha = P$	$z\tilde{t}\,\sin^2\theta + \frac{1}{2}U\,\cos^2\frac{1}{2}\theta$	$\cos^2\frac{1}{2}\theta$	-1

$H^{\mathrm{BdG}}_{\mathbf{k},\alpha}$ takes a particular form

$$H^{\mathrm{BdG}}_{\mathbf{k},\alpha} = \begin{bmatrix} \xi_\alpha + \lambda_\alpha H^{\mathrm{hop}}_{\mathbf{k}} & \zeta_\alpha\kappa_\alpha H^{\mathrm{hop}}_{\mathbf{k}} \\ \zeta_\alpha\kappa_\alpha H^{\mathrm{hop}}_{\mathbf{k}} & \xi_\alpha + \lambda_\alpha H^{\mathrm{hop}}_{\mathbf{k}} \end{bmatrix}, \tag{5}$$

with all parameters given in Table I. By making the Bogoliubov transformation (see Appendix C for details), one can obtain the excitation spectrum above the mean-field ground-state $\hat{H} \simeq \sum_{\mathbf{k},\lambda,\alpha=A,P} E_{\mathbf{k},\lambda,\alpha}\hat{\gamma}^\dagger_{\mathbf{k},\lambda,\alpha}\hat{\gamma}_{\mathbf{k},\lambda,\alpha}$, where λ is the band index, and a constant term is omitted.

To identify these excitation modes $\hat{\gamma}_{\mathbf{k},\lambda,\alpha}$ to be amplitude modes (Higgs modes) or phase modes (Goldstone modes), we study the time evolution after a small perturbation above the ground-state $|\Psi_{\mathbf{k},\lambda,\alpha}(t)\rangle = e^{-i\hat{H}t}(|G\rangle + \epsilon\hat{\gamma}^\dagger_{\mathbf{k},\lambda,\alpha}|G\rangle)$ with $\epsilon \ll 1$. In particular, fluctuation of the order parameters $\delta\varphi(t) = \langle\Psi_{\mathbf{k},\lambda,\alpha}(t)|\hat{a}_i|\Psi_{\mathbf{k},\lambda,\alpha}(t)\rangle - \langle G|\hat{a}_i|G\rangle$ to the leading order in ϵ is found to be

$$\delta\varphi(t) \propto \delta\varphi_{\mathrm{R}}\cos(E_{\mathbf{k},\lambda,\alpha}t) + i\,\delta\varphi_{\mathrm{I}}\sin(E_{\mathbf{k},\lambda,\alpha}t), \tag{6}$$

where $\delta\varphi_{\mathrm{R,I}} = \langle G|\hat{\gamma}_{\mathbf{k},\lambda,\alpha}\hat{a}_i \pm \hat{a}_i\hat{\gamma}^\dagger_{\mathbf{k},\lambda,\alpha}|G\rangle$ (see Appendix D for a detailed derivation). Without loss of generality, we can choose the order parameter to be real. Then, if $\delta\varphi(t)$ is real, the excitation is a pure amplitude mode; whereas if $\delta\varphi(t)$ is purely imaginary, the excitation is a pure phase mode. In general, the excitation could be a mixing of both such that the order parameter fluctuation $\delta\varphi(t)$ is a generic c number. Therefore, we define a flatness parameter,

$$F = \frac{|\delta\varphi_{\mathrm{R}}| - |\delta\varphi_{\mathrm{I}}|}{|\delta\varphi_{\mathrm{R}}| + |\delta\varphi_{\mathrm{I}}|} \in [-1, 1], \tag{7}$$

to quantify the amplitude and phase components of an excitation. A positive (negative) flatness indicates dominant amplitude (phase) character. A pure amplitude (phase) oscillation corresponds to $F = 1(-1)$. In the large filling limit, by calculating the flatness explicitly, we analytically find that $\hat{\gamma}_{\mathbf{k},\lambda,P}$ is a *pure* phase mode, and $\hat{\gamma}_{\mathbf{k},\lambda,A}$ is a *pure* amplitude mode (see Appendix D for details). In both Figs. 2 and 3 where we plot the low-energy excitation spectrum, the color scale of the plot shows the flatness calculated numerically: red (blue) points correspond to $F = 1(-1)$, respectively.

Excitations above the ground state are described by the quadratic Hamiltonian Eq. (4), thus, their topological character is obtained by analyzing the BdG matrix Eq. (5), which also obeys the inversion symmetry $\mathcal{I}_\tau H^{\mathrm{BdG}}_{-\mathbf{k},\alpha}\mathcal{I}^{-1}_\tau = H^{\mathrm{BdG}}_{\mathbf{k},\alpha}$, where $\mathcal{I}_\tau = \tau_0 \otimes \mathcal{I}$, and τ_0 is the two-by-two identity matrix acting on the Nambu space. We naturally generalize the polarization vector to a symplectic form [18], $\mathbf{P} = \int_{\mathrm{BZ}} \frac{d^2k}{(2\pi)^2}\mathbf{A}(\mathbf{k})$ where $\mathbf{A}(\mathbf{k}) = i\sum_{\lambda_1\leqslant\lambda\leqslant\lambda_2}\mathrm{Tr}(\Gamma_\lambda W^{-1}_{\mathbf{k}}\partial_{\mathbf{k}}W_{\mathbf{k}})$, Γ_λ projects to the λth band, and the pseudounitary matrix $W_{\mathbf{k}}$ diagonalizes $H^{\mathrm{BdG}}_{\mathbf{k},\alpha}$. Each component of $\mathbf{P}$ is quantized to a $\mathbb{Z}_2$ number (see Appendix E for a proof), $P_\mu = \frac{1}{2}[(\sum_{\lambda_1\leqslant\lambda\leqslant\lambda_2} n_{\lambda,\mu}) \mod 2]$, where $(-1)^{n_{\lambda,\mu}} = \eta_\lambda(\mathbf{X}_\mu)\eta_\lambda(\mathbf{\Gamma})$ and η is the eigenvalue of the generalized inversion operator $\mathcal{I}_\tau$. In the large filling limit, one can explicitly polar decompose the Bogoliubov transformation matrix $W_{\mathbf{k},\alpha}$ as the product of a unitary matrix and a Hermitian (also pseudounitary) matrix. It then follows straightforwardly that (see Appendix E for a proof)

$$W^{-1}_{\mathbf{k}_{\mathrm{inv}}}\mathcal{I}_\tau W_{\mathbf{k}_{\mathrm{inv}}} = \tau_0 \otimes \left(Q^{-1}_{\mathbf{k}_{\mathrm{inv}}}\mathcal{I}Q_{\mathbf{k}_{\mathrm{inv}}}\right),$$

where $Q_{\mathbf{k}}$ is the unitary matrix that diagonalizes $H^{\mathrm{hop}}_{\mathbf{k}}$. Namely, the parity eigenvalues of both the Higgs bands and the Goldstone bands at inversion symmetric momenta are *identical* to the noninteracting bands. Consequently, not only the Goldstone bands, but also the Higgs bands inherit the topology of the background noninteracting bands: When $t_1 < t_2$ ($t_1 > t_2$) both of them are topologically nontrivial (trivial) with symplectic polarization vector $\mathbf{P} = (1/2, 1/2)$ [$\mathbf{P} = (0, 0)$]. We then confirm the bulk-boundary correspondence numerically by calculating the excitation spectrum in a ribbon geometry and, indeed, observe the edge states in the topologically nontrivial regime as shown in Fig. 2. The flatness for these two types of modes are also calculated numerically,

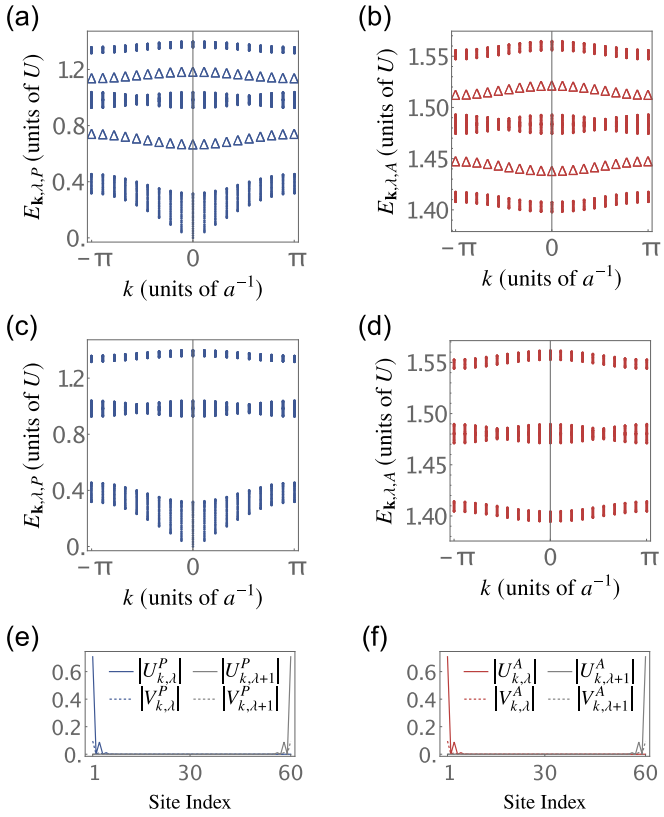

FIG. 2. Excitation spectrum of the 2D SSH-BHM in a ribbon geometry in the large filling limit for $\tilde{t} = 3U/16$. (a) ($t_1/t_2 = 1/8$) and (c) ($t_1/t_2 = 8$) are the Goldstone phase modes. (b) ($t_1/t_2 = 1/8$) and (d) ($t_1/t_2 = 8$) are the Higgs amplitude modes. Bulk modes are shown by solid dots, whereas topological edge modes are shown by triangles. All modes are doubly degenerate due to inversion symmetry. (e) and (f) are typical wave functions of topological edge modes for phase modes and amplitude modes, respectively. And the gray lines are their inversion symmetric partners.

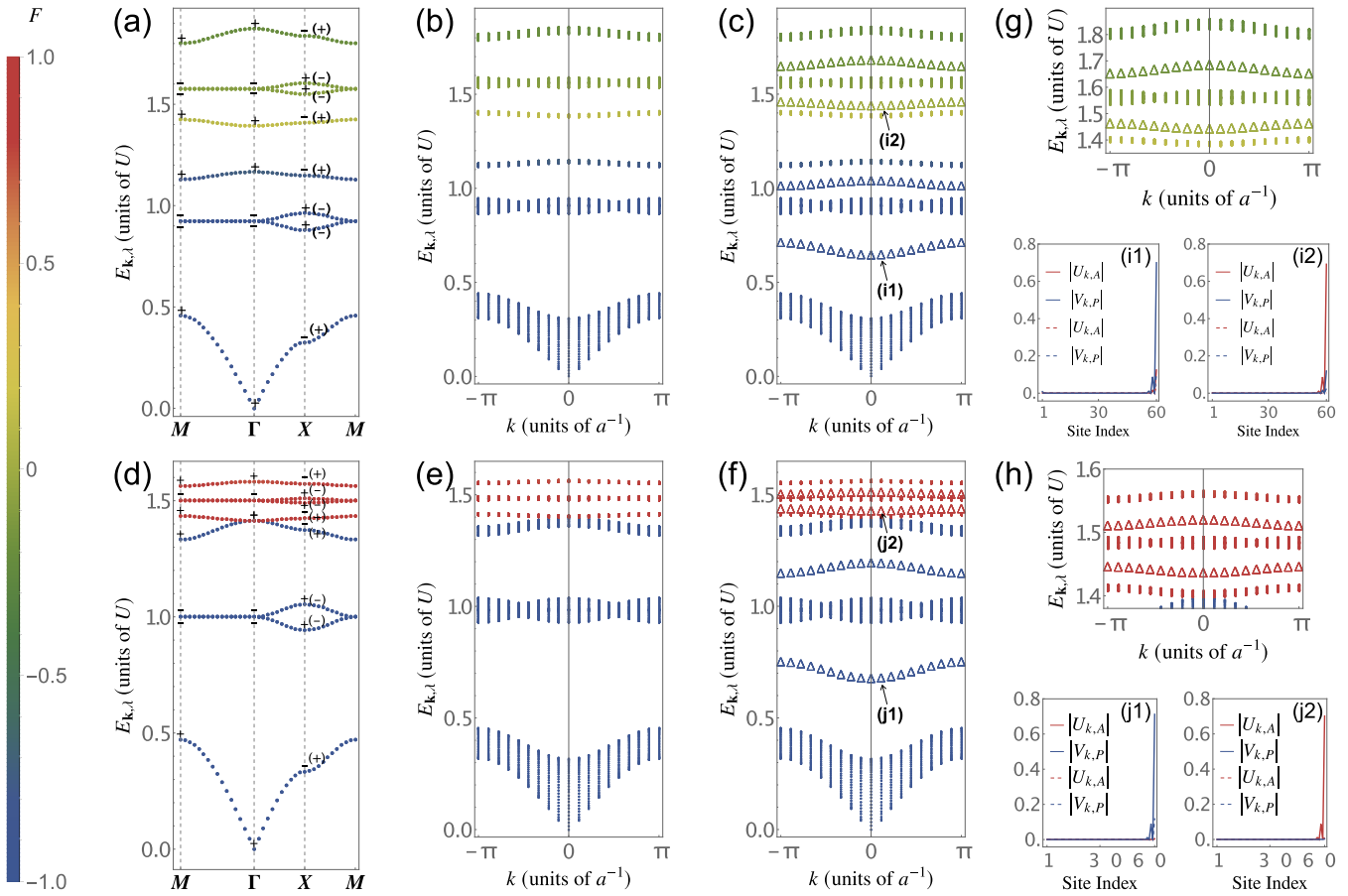

FIG. 3. Excitation spectrum of the 2D SSH-BHM under PBCs (a) and (d) and in a ribbon geometry (b), (c), (e), and (f) at filling $q = 1$ for (a)–(c) and $q = 50$ for (d)–(f) for $\tilde{t} = 3U/16$ with color code indicating the flatness defined in Eq. (7). Bulk (topological edge) modes are plotted by dots (triangles) with typical wave functions shown in (i) and (j) (only one of the two degenerate modes is plotted). In (g) and (h) we zoom in on the excitation spectrums at high energies for (c) and (f), respectively.

shown by the color scale: red (blue) points correspond to $F = 1$ (-1), which is also in agreement with our analysis, reflecting the fact that they are fully decoupled in the large filling limit.

IV. FINITE FILLING CASE

The slave boson method also works at finite fillings, but now $\hat{a}_i^\dagger \simeq (\sqrt{q+1}\hat{b}_{i,q+1}^\dagger \hat{b}_{i,q} + \sqrt{q}\hat{b}_{i,q}^\dagger \hat{b}_{i,q-1})$, and the PH symmetric line is given by $\mu = (q-1/2) - [z\tilde{t} + (\sqrt{q+1}+\sqrt{q})^{-2}]/4$ (see Appendix A for the derivation), which is bent downwards due to asymmetric Bose enhancement. The resulting excitation spectrum for open (OBCs) and periodic (PBCs) boundary conditions are given in Fig. 3, which shows that the flatness is between -1 and $+1$, in general, due to off-diagonal coupling terms between the Goldstone mode and the Higgs mode. When we increase the filling, this coupling becomes weaker such that the flatness tends to ± 1. Despite the absence of pure phase-amplitude character, we can still identify a topological character since $H_{\mathbf{k}}^{(2)}$ in Eq. (4) obeys an inversion symmetry at any fillings, and the bulk topological index is well defined. By examining the parity eigenvalues at the inversion symmetric momenta, labeled in Figs. 3(a) and 3(d), we find that these excitation bands either phase or amplitude fluctuation dominated all inherit the topology of the background noninteracting bands, and they have the same topologically trivial-nontrivial transition point as the background bands. It follows that two groups of midgap edge states under OBCs are observed in Figs. 3(c) and 3(f). Their flatnesses, respectively, approaches ± 1 when increasing the filling. Thus, the coupling between the Higgs bands and the Goldstone bands will not break the topology of the excitation spectrum and the bulk-boundary correspondence.

V. EFFECTIVE ACTION ANALYSIS

Lastly we present a simple and unified picture for the results obtained so far. At an integer filling q, near the SF-MI phase transition, one can use a strong-coupling random-phase approximation [68] to arrive at an effective action for the 2D SSH-BHM,

$$S_{\text{eff}} = \int d\tau \left\{ \sum_i \left[a_i^* \left(\sum_{\ell=0}^{\infty} (-1)^{\ell+1} c_\ell \partial_\tau^\ell \right) a_i + \frac{\tilde{U}}{2} |a_i|^4 \right] - \sum_{ij} t_{ij} a_i^* a_j \right\}, \tag{8}$$

where all c_ℓ's are real, and $\tilde{U}$ is a renormalized interaction strength (see Appendix F for a detailed derivation). Note

this effective action is obtained by *two* successive Hubbard-Stratonovich transformations, and the auxiliary field a in Eq. (8) generates same correlators as the original bosonic field. In the SF phase, by introducing small fluctuations $a_i(\tau) = [\varphi + \delta\rho_i(\tau)]e^{i\,\delta\theta_i(t)}$, we expand Eq. (8) to quadratic order,

$$S^{(2)} = \int d\tau \sum_{ij} [\delta\rho_i \quad \delta\theta_i] \begin{bmatrix} t_{ij} - \sum_{n=0}^{\infty} c_{2n}\partial_\tau^{2n} - \tilde{\mu} + 3\tilde{U}\varphi^2 & i\,\delta_{ij}\varphi \sum_{n=0}^{\infty} c_{2n+1}\partial_\tau^{2n+1} \\ -i\,\delta_{ij}\varphi \sum_{n=0}^{\infty} c_{2n+1}\partial_\tau^{2n+1} & t_{ij} + \left(-\sum_{n=0}^{\infty} c_{2n}\partial_\tau^{2n} - \tilde{\mu} + \tilde{U}\varphi^2\right)\varphi^2 \end{bmatrix} \begin{bmatrix} \delta\rho_j \\ \delta\theta_j \end{bmatrix}. \tag{9}$$

By requiring $c_1 = 0$ (i.e., on the PH symmetric line) and in the low-energy limit $\omega \to 0$ (i.e., dropping all the higher-order time derivative terms), phase modes, and amplitude modes become decoupled, which explains the persistence of pure phase modes at low energies in Fig. 3 for all fillings. Noting that along the PH symmetric line, it is easy to show that $c_\ell \sim O(q^{-\ell+1})$ for $\ell \geqslant 2$, thus, in the large filling limit only c_2 survives, even away from the low-energy limit. Moreover, these modes inherit band topology directly from the 2D SSH model as the hopping terms are not altered. This explains the existence of topological Higgs-amplitude and Goldstone-phase bands for $q \to \infty$ in Fig. 2.

As a by-product, we point out that if the hopping term breaks time-reversal symmetry (TRS), i.e., t_{ij} is not purely real, one can easily show that there are off-diagonal terms entering Eq. (9), which is proportional to the imaginary part of t_{ij}. Thus, the amplitude modes and phase modes have nonvanishing coupling *even in the infinite filling limit*. This fact can also be derived from the slave boson picture [see discussions around Eq. (C8)]. Physically speaking, the so-called particle-hole symmetry indicates that the action Eq. (8) is invariant under the exchange $\psi \leftrightarrow \psi^*$, up to a total time derivative term. If $t_{ij} = t_{ji}^* \neq t_{ji}$, the hopping term cannot return to itself upon this exchange: $a_i^* t_{ij} a_j \to a_i t_{ij} a_j^* = a_i^* t_{ji} a_j \neq a_i^* t_{ij} a_j$ where repeated indices are summed over. Nevertheless, we predict that the mixed excitation spectrums still inherit the band topology and will exhibit two groups of midgap edge states under OBCs.

VI. DISCUSSION AND OUTLOOK

To summarize, the low-energy excitations of the two-dimensional SSH-BHM in both the infinite filling limit and the finite fillings at the particle-hole symmetry line are studied. Using the slave boson approach, we showed that, in the former case, the low-energy excitations consist of fully separated Goldstone modes and Higgs modes both of which inherent the topology from the underlying noninteracting bands. In the latter case, these modes become coupled, which is quantitatively characterized by the flatness defined in Eq. (7); nonetheless, their topological properties are not altered. We also numerically verified the bulk-boundary correspondence for both cases and showed that at a moderate filling the topological edge modes with dominated amplitude (phase) character emerge. Lastly, via an effective action analysis, we provide a universal physical picture for the topology of the Goldstone modes and Higgs modes not only unifies two results obtained in this paper, but also possibly applies to other symmetry-breaking systems, such as superconductors and quantum magnets.

Since the edge modes of Higgs type and Goldstone type illustrated in this ppaper are of topological origin, we expect that they are robust against disorder [69] that: (1) respect the inversion symmetry, (2) and is sufficiently weak so that topological excitation band gap does not close and the system does not enter into other possible phases, such as the Bose glass phase (where the topology of excitations may change dramatically). Ultimately, the fate and robustness of topological Higgs modes subject to disorder need future study. We note that similar works on other bosonic topological systems with disorder have been discussed recently [70,71].

Thanks to the fast development of experimental techniques, the Bragg spectroscopy [52] and the lattice-modulation spectroscopy [53] can detect the Higgs mode; and the box trap with a sharp boundary has been achieved in cold-atom systems [72]. We expect that the predicted topological Higgs amplitude edge modes can be observed as a sharp peak within the band gap in the spectroscopy. In this paper, our discussions are limited to the quadratic order so that there is no coupling between these modes. By including higher-order terms, interactions between the excitation modes can be considered. Then it is interesting to investigate the impacts of mode coupling on the stability of the highly localized Higgs and Goldstone edge excitations. It is also interesting to explore similar topological Higgs amplitude modes in other systems. Particularly, in quantum magnets, it is possible that the topological Higgs amplitude modes yield a nontrivial contribution to the thermal Hall effect, similar to those resulting from the topological magnons [73].

ACKNOWLEDGMENTS

We thank W. Yi, J. Zhang, and Z.-Y. Shi for helpful comments. Y.D. acknowledges support from the National Natural Science Foundation of China (under Grant No. 11625522) and the National Key R&D Program of China (under Grants No. 2016YFA0301604 and No. 2018YFA0306501).

APPENDIX A: MEAN-FIELD THEORY AND PHASE DIAGRAM

In this Appendix, we discuss the mean-field phase diagram of the d-dimensional SSH-BHM, which returns to the well-known phase diagram of the standard BHM upon setting $t = (t_1 + t_2)/2$ (for t_1/t_2 not far from unity).

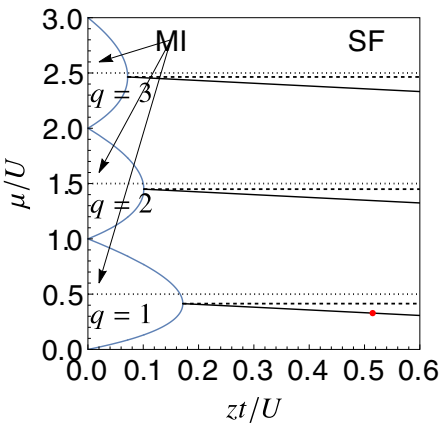

FIG. 4. Phase diagram of the dD SSH-BHM with blue lines separating the MI phase and the SF phase. It is the same as the standard BH model with the hopping parameter $t = (t_1 + t_2)/2$. Here the coordination number $z = 2d = 4$ for the 2D SSH-BHM. The black dotted horizontal lines start from each middle of the lobe. The black dashed horizontal lines start from each tip of the lobe. The black solid lines are integer filling lines in the SF phase obtained from Eq. (B7). We always set the chemical potential μ on these black solid lines where the excitations have the most visible phase-amplitude character. In particular, the red dot corresponds to the case in Figs. 3(a)– 3(c) the main text.

In the strong-coupling mean-field theory, one decouples the hopping term $-t_{ij}\hat{a}_i^\dagger\hat{a}_j$ as $-t_{ij}(\hat{a}_i^\dagger\phi_j + \hat{a}_j\phi_i^* - \phi_i^*\phi_j)$. Then the original Hamiltonian Eq. (1) given in the main text becomes

$$\hat{H} \approx \sum_i \hat{H}_i^{\mathrm{MF}} = \sum_i \Bigg[-\sum_j \left(\hat{a}_i^\dagger t_{ij}\phi_j - \frac{1}{2}t_{ij}\phi_i^*\phi_j + \mathrm{H.c.}\right) + \frac{1}{2}U\hat{n}_i(\hat{n}_i - 1) - \mu\hat{n}_i \Bigg], \tag{A1}$$

where $\phi_i = {}_i\langle\Phi_0|\hat{a}_i|\Phi_0\rangle_i$ and $|\Phi_0\rangle_i$ is the ground state of $\hat{H}_i^{\mathrm{MF}}$ obtained self-consistently. Note this approach is equivalent to introducing the Gutzwiller ansatz $|\Psi_{\mathrm{Gutzwiller}}\rangle = \bigotimes_i(\sum_n c_{i,n}|n\rangle_i)$, where $|n\rangle_i = (\hat{a}_i^\dagger)^n\sqrt{n!}|0\rangle$ ($|0\rangle$ is the vacuum of operator $\hat{a}$), and minimizing the variational ground-state energy $\langle\Psi_{\mathrm{Gutzwiller}}|\hat{H}|\Psi_{\mathrm{Gutzwiller}}\rangle$. Also note Eq. (A1) can be used for the system under OBCs in which case the order parameter ϕ_i is generally site dependent.

For the d-dimensional SSH-BHM, the hopping matrix t_{ij} is chosen staggered as t_1 and t_2 along all d directions. Under PBCs and assuming a site-independent real order parameter $\phi_i = \phi \in \mathbb{R}$, the mean-field Hamiltonian Eq. (A1) then reduces to

$$\hat{H}_i^{\mathrm{MF}} \approx \sum_i \left[-(zt\phi\hat{a}_j + \mathrm{H.c.}) + zt\phi^2 + \frac{1}{2}U\hat{n}_i(\hat{n}_i - 1) - \mu\hat{n}_i\right], \tag{A2}$$

where $z = 2d$ is the coordination number and $t = \frac{t_1+t_2}{2}$. Equation (A2) is precisely the strong-coupling mean-field Hamiltonian for the d-dimensional BH model [74], whose phase diagram is reviewed below.

Assuming the quantum phase transition being of second order, i.e., $\phi \ll 1$ near the transition boundary, one can treat $\hat{V} = -zt\phi\hat{a}_j + \mathrm{H.c.}$ as the perturbation to $\hat{H}_0 = zt\phi^2 + \frac{1}{2}U\hat{n}_i(\hat{n}_i - 1) - \mu\hat{n}_i$ in Eq. (A2). The unperturbed ground-state energy is then given by $\varepsilon_0^{(0)} = \frac{1}{2}Uq(q-1) - \mu q$ for $q = \lfloor\mu/U\rfloor + 1$ if $\mu > 0$ and $q = 0$, otherwise, with the unperturbed ground state being $|\Phi_0^{(0)}\rangle = |q\rangle$. The first-order correction vanishes by inspection. And the second-order correction is given by the standard formula [75] $\varepsilon_0^{(2)} = \sum_{l\neq 0}\frac{|\langle\varepsilon_0^{(0)}|\hat{V}|\epsilon_l^{(0)}\rangle|^2}{\varepsilon_0^{(0)} - \epsilon_l^{(0)}}$, which leads to $\varepsilon_0^{(2)} = (zt\phi)^2[\frac{q}{(q-1)-\mu} + \frac{q+1}{\mu - qU}]$. Thus, the ground-state energy reads $\varepsilon_0 = a_0 + a_2\phi^2 + O(\phi^4)$. According to Landau theory, phase transition occurs at $a_2 = (zt)^2[\frac{q}{(q-1)-\mu} + \frac{q+1}{\mu-qU}] + zt = 0$, whose solution gives the well-known lobe in the μ-zt phase diagram at filling q (we set $U = 1$ as the energy unit) [45],

$$\mu_\pm(q) = q - \frac{1}{2} - \frac{1}{2}zt \pm \frac{1}{2}\sqrt{(zt)^2 + 1 - 2zt(2q+1)}. \tag{A3}$$

The *tip* of the lobe corresponds to $\mu_+(q) = \mu_-(q)$, which leads to

$$(zt_c, \mu_c) = [1 + 2q - 2\sqrt{q(1+q)}, \sqrt{q(1+q)} - 1]. \tag{A4}$$

In the SF phase, we can numerically obtain the line of the integer filling factor near the qth lobe by setting ${}_i\langle\Phi_0|\hat{n}_i|\Phi_0\rangle_i = q$. It generally bends downward due to PH asymmetry at a finite filling. When truncated to only three local states, it has an analytical expression given in Eq. (B7). A typical phase diagram is shown in Fig. 4.

APPENDIX B: DERIVATION OF THE BOGOLIUBOV–DE GENNES HAMILTONIAN

In this Appendix, we derive the bosonic BdG Hamiltonian used in the main text. PBCs and a site-independent order parameter are assumed throughout; differences occurred in OBCs are mentioned in the end.

Focusing on the strongly coupled SF phase in the vicinity of the qth Mott lobe, only three local states,

$$|q-1\rangle_i, \quad |q\rangle_i, \quad |q+1\rangle_i, \tag{B1}$$

at each site i dominate the low-energy behavior of the system. Following Altman and Auerbach [47], we truncate the bosonic Fock space to these three states and introduce a Gutzwiller-type mean-field ground-state ansatz $|G\rangle = \otimes_i|\Phi_0\rangle_i$, where [48]

$$|\Phi_0\rangle_i = \cos(\theta/2)|q\rangle + \sin(\theta/2)[\cos(\chi/2)|q+1\rangle_i + \sin(\chi/2)|q-1\rangle_i]. \tag{B2}$$

Then the order parameter becomes

$$\phi = {}_i\langle\Phi_0|\hat{a}_i|\Phi_0\rangle_i = \frac{1}{2}\left(\sqrt{q+1}\cos\frac{\chi}{2} + \sqrt{q}\sin\frac{\chi}{2}\right)\sin\theta, \tag{B3}$$

and the variational ground-state energy per site is

$$\varepsilon_{\rm var}(\theta,\chi)=\frac{\langle G|\hat{H}|G\rangle}{N}$$
$$=\left[\frac{1}{2}-\delta\mu\,\cos\,\chi\right]\sin^2\frac{\theta}{2}-\frac{z\tilde{t}}{2}\left[1+\sqrt{1+q^{-1}}\,\sin\,\chi+\frac{1}{2q}(1+\cos\,\chi)\right]\sin^2\theta+\text{const.}, \tag{B4}$$

where N is the number of lattice sites, two parameters $\tilde{t}=qt$ and $\delta\mu=\mu-(q-1/2)$ are the renormalized hopping strength and the chemical potential measured from the *middle* of the lobe, respectively. Minimizing Eq. (B4) with respect to χ at a fixed θ, namely, setting $\partial_\chi\varepsilon_{\rm var}(\theta,\chi)=0$, one obtains

$$\chi(\theta)=\arctan\left[\frac{2z\tilde{t}(1+\cos\,\theta)\sqrt{q(q+1)}}{z\tilde{t}+\frac{4}{q}\delta\mu+z\tilde{t}\,\cos\,\theta}\right]. \tag{B5}$$

Further setting $\partial_\theta\varepsilon_{\rm var}(\theta,\chi)=0$ and using Eq. (B5), one can find the mean-field solution $\bar{\theta}$, whose explicit expression is lengthy and omitted. Note by expanding $\partial_\theta\varepsilon_{\rm var}[\theta,\chi(\theta)]$ around $\theta=0$ as $\partial_\theta\varepsilon_{\rm var}[\theta,\chi(\theta)]=\text{const.}+\tilde{a}_2\theta+O(\theta^2)$, where

$$\tilde{a}_2=-\frac{1}{4}\left\{2\delta\mu\sqrt{\frac{4q(q+1)(zt)^2}{(2\delta\mu+zt)^2}+1}+zt\left(\sqrt{\frac{4q(q+1)(zt)^2}{(2\delta\mu+zt)^2}+1}+2q+1\right)-1\right\}, \tag{B6}$$

and setting $\tilde{a}_2=0$, one again finds the phase boundary which is in agreement with Eq. (A3).

Within this approximation, one can also obtain the integer filling line in the SF phase analytically. Namely, from ${}_i\langle\Phi_0|\hat{n}_i|\Phi_0\rangle_i=q+\cos\,\bar{\chi}\,\sin^2(\bar{\theta}/2)$, the integer filling condition means $\chi=\pi/2$. Thus, Eq. (B5) leads to $\bar{\theta}=\arccos\frac{-z\tilde{t}-4\delta\mu}{z\tilde{t}}$. One then solve $[\partial_\theta\varepsilon_{\rm var}(\theta,\pi/2)]|_{\theta=\bar{\theta}}$ to get

$$\delta\mu_{\rm phs}=-\frac{1}{4}[z\tilde{t}+(\sqrt{q+1}+\sqrt{q})^{-2}], \tag{B7}$$

which is bent down due to asymmetric Bose enhancement at finite fillings. It is this line we refer to as the PH symmetric line.

We define three commuting bosonic operators that create three Fock states at a given site i, $b^\dagger_{i,\ell}|\text{vac}\rangle=|q+\ell\rangle_i$, $\ell=0,\pm1$. They must satisfy the local constraint $\sum_{\ell=-1}^{1}b^\dagger_{i,\ell}b_{i,\ell}=1$. Then the original bosonic creation operator can be expressed as $\hat{a}^\dagger_i=\sum_{\ell,\ell'}{}_i\langle q+\ell|\hat{a}^\dagger_i|q+\ell'\rangle_i\hat{b}^\dagger_{i,\ell}\hat{b}_{i,\ell'}=\sqrt{q+1}\hat{b}^\dagger_{i,1}\hat{b}_{i,0}+\sqrt{q}\hat{b}^\dagger_{i,0}\hat{b}_{i,-1}$, and the strong-coupling mean-field Hamiltonian Eq. (A2) becomes (up to a constant)

$$\hat{H}^{\rm MF}_i=[\hat{b}^\dagger_{i,-1}\quad\hat{b}^\dagger_{i,0}\quad\hat{b}^\dagger_{i,1}]H\begin{bmatrix}\hat{b}_{i,-1}\\ \hat{b}_{i,0}\\ \hat{b}_{i,1}\end{bmatrix}, \tag{B8}$$

where

$$H=\begin{bmatrix}\frac{1}{2}+\delta\mu+zt\phi^2 & -\sqrt{q}zt\phi & 0\\ -\sqrt{q}zt\phi & zt\phi^2 & -\sqrt{q+1}zt\phi\\ 0 & -\sqrt{q+1}zt\phi & \frac{1}{2}-\delta\mu+zt\phi^2\end{bmatrix}. \tag{B9}$$

Equation (B8) is diagonalized by the following rotation:

$$\begin{bmatrix}\hat{\beta}_{i,0}\\ \hat{\beta}_{i,1}\\ \hat{\beta}_{i,2}\end{bmatrix}=T(\alpha)\begin{bmatrix}\hat{b}_{i,-1}\\ \hat{b}_{i,0}\\ \hat{b}_{i,1}\end{bmatrix}, \tag{B10}$$

where

$$T(\alpha)=\begin{pmatrix}\sin\left(\frac{\bar{\theta}}{2}\right)\sin\left(\frac{\bar{\chi}}{2}\right) & \cos\left(\frac{\bar{\theta}}{2}\right) & \sin\left(\frac{\bar{\theta}}{2}\right)\cos\left(\frac{\bar{\chi}}{2}\right)\\ \cos(\alpha)\cos\left(\frac{\bar{\theta}}{2}\right)\sin\left(\frac{\bar{\chi}}{2}\right)+\sin(\alpha)\cos\left(\frac{\bar{\chi}}{2}\right) & -\cos(\alpha)\sin\left(\frac{\bar{\theta}}{2}\right) & \cos(\alpha)\cos\left(\frac{\bar{\theta}}{2}\right)\cos\left(\frac{\bar{\chi}}{2}\right)-\sin(\alpha)\sin\left(\frac{\bar{\chi}}{2}\right)\\ \cos(\alpha)\cos\left(\frac{\bar{\chi}}{2}\right)-\sin(\alpha)\cos\left(\frac{\bar{\theta}}{2}\right)\sin\left(\frac{\bar{\chi}}{2}\right) & \sin(\alpha)\sin\left(\frac{\bar{\theta}}{2}\right) & -\sin(\alpha)\cos\left(\frac{\bar{\theta}}{2}\right)\cos\left(\frac{\bar{\chi}}{2}\right)-\cos(\alpha)\sin\left(\frac{\bar{\chi}}{2}\right)\end{pmatrix}, \tag{B11}$$

with $\bar{\chi}=\chi(\bar{\theta})$. The rotation angle α is determined by requiring that $THT^\dagger=\text{diag}(\varepsilon_0,\varepsilon_1,\varepsilon_2)$. It can be shown straightforwardly that $(THT^\dagger)_{12}=(THT^\dagger)_{13}=0$ always holds; one only needs to set $(THT^\dagger)_{23}=0$, which leads to

$$\bar{\alpha}=\frac{2\,\cos\left(\frac{\bar{\theta}}{2}\right)\{\sin(\bar{\chi})[zt\,\cos(\bar{\theta})+4\delta\mu-zt]-2\sqrt{q}\sqrt{q+1}zt[\cos(\bar{\theta})-1]\cos(\bar{\chi})\}}{\cos(\bar{\theta})[1-2\delta\mu\,\cos(\bar{\chi})]+zt\,\sin^2(\bar{\theta})[2\sqrt{q}\sqrt{q+1}\,\sin(\bar{\chi})+2q+1]+\cos(\bar{\chi})[zt\,\sin^2(\bar{\theta})-6\delta\mu]-1}. \tag{B12}$$

Note the rotated operators also satisfy the local constraint as before, and the local eigenstates are now given by $|\Phi_\sigma\rangle_i = \beta^\dagger_{i,\sigma}|\text{vac}\rangle$ for $\sigma = 0$–2. Here $\sigma = 0$ modes is the local ground state, and $\sigma = 1, 2$ modes are two local excitations.

In terms of the rotated operators $\hat{\beta}$, Eq. (1) given in the main text can be recast as

$$\hat{H} = -\sum_{ij}\sum_{\alpha\sigma\gamma\delta}\mathcal{A}_{\sigma\alpha}\mathcal{A}_{\gamma\delta}t_{ij}\beta^\dagger_{i\alpha}\beta_{i\sigma}\beta^\dagger_{j\gamma}\beta_{j\delta} + \sum_i\sum_{\alpha\sigma}\langle\Phi_\alpha|\left[\frac{1}{2}U\hat{n}_i(\hat{n}_i-1) - \mu\hat{n}_i\right]|\Phi_\sigma\rangle\beta^\dagger_{i\alpha}\beta_{i\sigma}, \tag{B13}$$

where $\mathcal{A}_{\alpha\sigma} = {}_i\langle\Phi_\alpha|\hat{a}^\dagger_i|\Phi_\sigma\rangle_i$. Note we have used the fact that $\mathcal{A}_{\alpha\sigma}$ is real, hence, ${}_i\langle\Phi_\alpha|\hat{a}^\dagger_i|\Phi_\sigma\rangle_i = {}_i\langle\Phi_\sigma|\hat{a}_i|\Phi_\alpha\rangle_i$. By treating $\hat{\beta}$ operators as classical fields, the energy minimum is reached for $\beta^*_0 = \beta_0 = 1$ when all other modes vanish. We perform a harmonic expansion of Eq. (B13) around this saddle point by condensing operators $\hat{\beta}^{(\dagger)}_0$,

$$\hat{\beta}^{(\dagger)}_{i,0} \to \sqrt{1 - \sum_{\sigma>0}\hat{\beta}^\dagger_{i,\sigma}\hat{\beta}_{i,\sigma}} \approx 1 - \frac{1}{2}\sum_{\sigma>0}\hat{\beta}^\dagger_{i,\sigma}\hat{\beta}_{i,\sigma}. \tag{B14}$$

The zeroth-order term gives the mean-field ground-state energy $H^{(0)} = \langle G|\hat{H}|G\rangle$. The first-order term can be rearranged as $\hat{H}^{(1)} = \sum_i\sum_{\alpha>0}\hat{\beta}_{i\alpha}\,{}_i\langle\Phi_0|\hat{H}^{\text{MF}}_i|\Phi_\alpha\rangle_i + \text{H.c.}$, which vanishes identically due to orthogonality between local eigenstates $|\Phi_0\rangle_i$ and $|\Phi_\sigma\rangle_i$ for $\sigma > 0$. The second-order term reads

$$\hat{H}^{(2)} = \hat{H}_\text{h} + \hat{H}_\text{p} + \hat{H}_\text{o}, \tag{B15}$$

where

$$\hat{H}_\text{h} = -\sum_{ij}\sum_{\alpha,\sigma>0}(\mathcal{A}_{0\alpha}\mathcal{A}_{0\sigma}t_{ij} + A_{\alpha0}\mathcal{A}_{\sigma0}t_{ji})\hat{\beta}^\dagger_{i\alpha}\hat{\beta}_{j\sigma}, \tag{B16a}$$

$$\hat{H}_\text{p} = -\frac{1}{2}\sum_{ij}\sum_{\alpha,\sigma>0}(\mathcal{A}_{0\alpha}\mathcal{A}_{\sigma0}t_{ij} + \mathcal{A}_{\alpha0}\mathcal{A}_{0\sigma}t_{ji})\hat{\beta}^\dagger_{i\alpha}\hat{\beta}^\dagger_{j\sigma} + \text{H.c.}, \tag{B16b}$$

$$\hat{H}_\text{o} = \sum_i\sum_{\alpha,\sigma>0}(\varepsilon_\alpha - \varepsilon_0)\hat{\beta}^\dagger_{i\alpha}\hat{\beta}_{i\alpha}, \tag{B16c}$$

corresponding to hopping, pairing, and on-site terms, respectively. Note, since $\mathcal{A}_{\alpha0}$ is generally nonzero, the hopping and pairing terms will couple two local excitation modes. In momentum space, Eq. (B16) becomes

$$\hat{H}_\text{h} = \sum_{\mathbf{k}}\sum_{\alpha,\sigma>0}\sum_{\eta\eta'}\left[\mathcal{A}_{0\alpha}\mathcal{A}_{0\sigma}\left(H^\text{hop}_{\mathbf{k}}\right)_{\eta\eta'} + \mathcal{A}_{\alpha0}\mathcal{A}_{\sigma0}\left(H^{\text{hop}*}_{-\mathbf{k}}\right)_{\eta\eta'}\right]\hat{\beta}^\dagger_{\mathbf{k},\alpha\eta}\hat{\beta}_{\mathbf{k},\sigma\eta'}, \tag{B17a}$$

$$\hat{H}_\text{p} = \frac{1}{2}\sum_{\mathbf{k}}\sum_{\alpha,\sigma>0}\sum_{\eta\eta'}\left[\mathcal{A}_{0\alpha}\mathcal{A}_{\sigma0}\left(H^\text{hop}_{\mathbf{k}}\right)_{\eta\eta'} + \mathcal{A}_{\alpha0}\mathcal{A}_{0\sigma}\left(H^{\text{hop}*}_{-\mathbf{k}}\right)_{\eta\eta'}\right]\hat{\beta}^\dagger_{\mathbf{k},\alpha\eta}\hat{\beta}^\dagger_{-\mathbf{k},\sigma\eta'} + \text{H.c.}, \tag{B17b}$$

$$\hat{H}_\text{o} = \sum_{\mathbf{k}}\sum_{\alpha>0}\sum_{\eta\eta'}(\varepsilon_\alpha - \varepsilon_0)\hat{\beta}^\dagger_{\mathbf{k},\alpha\eta}\hat{\beta}_{\mathbf{k},\alpha\eta'}, \tag{B17c}$$

where η, η' are sublattice indices (assuming total n_s sublattices) and we have assumed that the hopping matrix t_{ij} is Hermitian, i.e., $t_{ji} = t^*_{ij}$. Here $H^\text{hop}_{\mathbf{k}}$ is the Bloch Hamiltonian of the hopping term, specifically, for the two-dimensional SSH model with four sublattices $n_s = 4$ as shown in Fig. 1 of the main text, it is

$$H^\text{hop}_{\mathbf{k}} = -\begin{pmatrix} 0 & t_1 + t_2e^{-ik_y} & t_1 + t_2e^{-ik_x} & 0 \\ t_1 + t_2e^{ik_y} & 0 & 0 & t_1 + t_2e^{-ik_x} \\ t_1 + t_2e^{ik_x} & 0 & 0 & t_1 + t_2e^{-ik_y} \\ 0 & t_1 + t_2e^{ik_x} & t_1 + t_2e^{ik_y} & 0 \end{pmatrix}. \tag{B18}$$

By arranging $\beta_{\mathbf{k},\alpha\eta}$ into a vector $\boldsymbol{\beta}_{\mathbf{k}}$, and defining two $2n_s \times 2n_s$ matrices $A_{\mathbf{k}}$ and $B_{\mathbf{k}}$ with components,

$$(A_{\mathbf{k}})_{\alpha\eta,\sigma\eta'} = \mathcal{A}_{0\alpha}\mathcal{A}_{0\sigma}\left(H^\text{hop}_{\mathbf{k}}\right)_{\eta\eta'} + \mathcal{A}_{\alpha0}\mathcal{A}_{\sigma0}\left(H^{\text{hop}*}_{-\mathbf{k}}\right)_{\eta\eta'} + (\varepsilon_\alpha - \varepsilon_0)\delta_{\eta\eta'}, \tag{B19a}$$

$$(B_{\mathbf{k}})_{\alpha\eta,\sigma\eta'} = \mathcal{A}_{0\alpha}\mathcal{A}_{\sigma0}\left(H^\text{hop}_{\mathbf{k}}\right)_{\eta\eta'} + \mathcal{A}_{\alpha0}\mathcal{A}_{0\sigma}\left(H^{\text{hop}*}_{-\mathbf{k}}\right)_{\eta\eta'}, \tag{B19b}$$

Eq. (B15) can be written compactly in a BdG form as

$$\hat{H}^{(2)} = \frac{1}{2}\sum_{\mathbf{k}}[\boldsymbol{\beta}^\dagger_{\mathbf{k}} \quad \boldsymbol{\beta}_{-\mathbf{k}}]H^\text{BdG}_{\mathbf{k}}\begin{bmatrix}\boldsymbol{\beta}_{\mathbf{k}} \\ \boldsymbol{\beta}^\dagger_{-\mathbf{k}}\end{bmatrix}, \tag{B20}$$

where

$$H_{\mathbf{k}}^{\mathrm{BdG}} = \begin{bmatrix} A_{\mathbf{k}} & B_{\mathbf{k}} \\ B_{-\mathbf{k}}^{*} & A_{-\mathbf{k}}^{T} \end{bmatrix}. \tag{B21}$$

For models with TRS,

$$H_{\mathbf{k}}^{\mathrm{hop}} = H_{-\mathbf{k}}^{\mathrm{hop}*}, \tag{B22}$$

Eq. (B19) simplifies to

$$A = F \otimes H_{\mathbf{k}}^{\mathrm{hop}} + \mathcal{E} \otimes I_{n_s}, \tag{B23a}$$

$$B = G \otimes H_{\mathbf{k}}^{\mathrm{hop}}, \tag{B23b}$$

where

$$F_{\alpha\sigma} = \mathcal{A}_{0\alpha}\mathcal{A}_{0\sigma} + \mathcal{A}_{\alpha 0}\mathcal{A}_{\sigma 0}, \tag{B24a}$$

$$G_{\alpha\sigma} = \mathcal{A}_{0\alpha}\mathcal{A}_{\sigma 0} + \mathcal{A}_{\alpha 0}\mathcal{A}_{0\sigma}, \tag{B24b}$$

$$\mathcal{E}_{\alpha\sigma} = \delta_{\alpha\sigma}(\varepsilon_{\alpha} - \varepsilon_{0}) \tag{B24c}$$

are two-by-two, real symmetric matrices in local excitation space, and I_{n_s} is the identity matrix in sublattice space.

Under OBCs, the order parameter becomes site dependent, and the mean-field theory has to be worked out numerically in a self-consistent manner from Eq. (A1). Then the physical boson annihilation operator in the rotated local basis $\mathcal{A}_i$ and local eigenenergies $\varepsilon_{i\alpha}$, $\alpha = 1$–3 become site dependent. Taking into account these differences, the quadratic Hamiltonian Eq. (B15) can still be solved by a Bogoliubov transformation. In our numerics, for simplicity, we reuse the order parameter obtained from PBCs. This leads to a tiny gap near zero energy for the excitations, which is manually removed by a shift of chemical potential as in Ref. [22]. We have numerically checked that this gap tends to zero as we enlarge the system size. Moreover, topological properties of the highly excited states are not affected anyway.

APPENDIX C: DIAGONALIZATION OF THE BdG HAMILTONIAN

In this Appendix, we first review the process of diagonalization of a generic bosonic BdG Hamiltonian, which also serves to introduce notations and set the stage for the discussion in the following appendices. Then we show that in the large filling limit, this Bogoliubov transformation can be constructed analytically. In particular, we explicitly show that the coupling between phase modes and amplitude modes only vanish when the noninteracting Hamiltonian has TRS, even in the large filling limit. We only discuss the momentum space version, the real space version can be formulated similarly.

1. The general case

A generic bosonic BdG Hamiltonian as given in Eq. (B21) is diagonalized by a Bogoliubov transformation,

$$W_{\mathbf{k}}^{\dagger} H_{\mathbf{k}}^{\mathrm{BdG}} W_{\mathbf{k}} = D_{\mathbf{k}} = \tau_0 \otimes \begin{bmatrix} E_{1,\mathbf{k}} & & \\ & E_{2,\mathbf{k}} & \\ & & \ddots \end{bmatrix}, \tag{C1}$$

where from here on τ_0 and $\tau_{1\text{–}3}$ denote a two-by-two identity matrix and Pauli matrices acting on the Nambu space, and

$$W_{\mathbf{k}} = \begin{bmatrix} U_{\mathbf{k}} & V_{-\mathbf{k}}^{*} \\ V_{\mathbf{k}} & U_{-\mathbf{k}}^{*} \end{bmatrix} \tag{C2}$$

is a pseudounitary matrix satisfying,

$$W_{\mathbf{k}}^{\dagger}\Sigma_3 W_{\mathbf{k}} = \Sigma_3 \quad \text{and} \quad W_{\mathbf{k}}\Sigma_3 W_{\mathbf{k}}^{\dagger} = \Sigma_3. \tag{C3}$$

We define the Bogoliubov quasiparticle annihilation operator via $\vec{\boldsymbol{\beta}}_{\mathbf{k}} = W_{\mathbf{k}}\vec{\boldsymbol{\gamma}}_{\mathbf{k}}$, where $\vec{\boldsymbol{\beta}}_{\mathbf{k}} = (\boldsymbol{\beta}_{\mathbf{k}}, \boldsymbol{\beta}_{-\mathbf{k}}^{\dagger})^{T}$. More explicitly,

$$\boldsymbol{\beta}_{\mathbf{k}} = U_{\mathbf{k}}\boldsymbol{\gamma}_{\mathbf{k}} + V_{-\mathbf{k}}^{*}\boldsymbol{\gamma}_{-\mathbf{k}}^{\dagger} \quad \text{and} \quad \boldsymbol{\beta}_{\mathbf{k}}^{\dagger} = V_{-\mathbf{k}}\boldsymbol{\gamma}_{-\mathbf{k}} + U_{\mathbf{k}}^{*}\boldsymbol{\gamma}_{\mathbf{k}}^{\dagger}. \tag{C4}$$

Then Eq. (B20) after this Bogoliubov transformation becomes

$$\hat{H}^{(2)} = \frac{1}{2}\sum_{\mathbf{k}} \vec{\boldsymbol{\beta}}_{\mathbf{k}}^{\dagger} H_{\mathbf{k}}^{\mathrm{BdG}} \vec{\boldsymbol{\beta}}_{\mathbf{k}} = \frac{1}{2}\sum_{\mathbf{k}} \vec{\boldsymbol{\gamma}}_{\mathbf{k}}^{\dagger} W_{\mathbf{k}}^{\dagger} H_{\mathbf{k}}^{\mathrm{BdG}} W_{\mathbf{k}} \vec{\boldsymbol{\gamma}}_{\mathbf{k}} = \sum_{\mathbf{k},\lambda} \left(E_{\lambda} + \frac{1}{2}\right) \gamma_{\mathbf{k}\lambda}^{\dagger}\gamma_{\mathbf{k}\lambda}, \tag{C5}$$

where λ is the band index. Generally, this Bogoliubov transformation has to be performed numerically.

2. Analytical solution at the large filling limit

First, we note that in the large filling limit $q \gg 1$ the original Hamiltonian Eq. (1) in the main text when truncated to three local states Eq. (B1) can be mapped to a bond-staggered XY model with uniaxial single-ion anisotropy and magnetic coupling [47], $\hat{H} \sim \sum_{i,j} \tilde{t}_{ij}(\hat{S}_i^x\hat{S}_j^x + \hat{S}_i^y\hat{S}_j^y) + \sum_i [\frac{1}{2}U(\hat{S}_i^z)^2 - \delta\mu\hat{S}_i^z]$, where $\langle i, j\rangle$ denotes nearest neighbors and $\tilde{t}_{ij} = pt_{ij}$. In the following, we will focus on the PH symmetric line, i.e., $\delta\mu = 0$. When taking $q \gg 1$, Eq. (B5) becomes $\chi = \pi/2$, and Eq. (B4) becomes $\varepsilon_{\mathrm{var}} = \frac{1}{2}(\sin^2\frac{\theta}{2} - z\tilde{t}\,\sin^2\theta)$. Its minimization leads to $\bar{\theta} = \arccos\frac{U}{4qzt}$ if $U < 4qzt$, and $\bar{\theta} = 0$ otherwise. Then the rotation angle $\bar{\alpha}$ given in Eq. (B12) reduces to $\bar{\alpha} = 0$. Thus, the unitary matrix T is

$$T(\bar{\theta}) = \frac{1}{\sqrt{2}} \begin{bmatrix} \sin\frac{\bar{\theta}}{2} & \sqrt{2}\cos\frac{\bar{\theta}}{2} & \sin\frac{\bar{\theta}}{2} \\ \cos\frac{\bar{\theta}}{2} & -\sqrt{2}\sin\frac{\bar{\theta}}{2} & \cos\frac{\bar{\theta}}{2} \\ 1 & 0 & -1 \end{bmatrix}. \tag{C6}$$

And the physical boson annihilation operator in this rotated basis is

$$\mathcal{A}_i \approx T \begin{bmatrix} 0 & \sqrt{q} & 0 \\ 0 & 0 & \sqrt{q} \\ 0 & 0 & 0 \end{bmatrix} T^\dagger = \sqrt{\frac{q}{2}} \begin{bmatrix} \sin\bar{\theta} & \cos\bar{\theta} & -\cos\frac{\bar{\theta}}{2} \\ \cos\bar{\theta} & -\sin\bar{\theta} & \sin\frac{\bar{\theta}}{2} \\ \cos\frac{\bar{\theta}}{2} & -\sin\frac{\bar{\theta}}{2} & 0 \end{bmatrix}. \tag{C7}$$

Then $\hat{H}_\mathrm{h}$ and $\hat{H}_\mathrm{p}$ defined in Eq. (B17) becomes

$$\hat{H}_\mathrm{h} = \frac{q}{2} \sum_{\mathbf{k}} \boldsymbol{\beta}_{\mathbf{k}}^\dagger \begin{bmatrix} \left(H_{\mathbf{k}}^{\mathrm{hop}} + H_{-\mathbf{k}}^{\mathrm{hop}*}\right)\cos^2\theta & \left(-H_{\mathbf{k}}^{\mathrm{hop}} + H_{-\mathbf{k}}^{\mathrm{hop}*}\right)\cos\frac{\theta}{2}\cos\theta \\ \left(-H_{\mathbf{k}}^{\mathrm{hop}} + H_{-\mathbf{k}}^{\mathrm{hop}*}\right)\cos\frac{\theta}{2} & \frac{1}{2}\left(H_{\mathbf{k}}^{\mathrm{hop}} + H_{-\mathbf{k}}^{\mathrm{hop}*}\right)\cos^2\frac{\theta}{2} \end{bmatrix} \boldsymbol{\beta}_{\mathbf{k}}, \tag{C8a}$$

$$\hat{H}_\mathrm{p} = \frac{q}{4} \sum_{\mathbf{k}} \boldsymbol{\beta}_{\mathbf{k}}^\dagger \begin{bmatrix} \left(H_{\mathbf{k}}^{\mathrm{hop}} + H_{-\mathbf{k}}^{\mathrm{hop}*}\right)\cos^2\theta & \left(H_{\mathbf{k}}^{\mathrm{hop}} - H_{-\mathbf{k}}^{\mathrm{hop}*}\right)\cos\frac{\theta}{2}\cos\theta \\ \left(H_{\mathbf{k}}^{\mathrm{hop}} - H_{-\mathbf{k}}^{\mathrm{hop}*}\right)\cos\frac{\theta}{2} & -\frac{1}{2}\left(H_{\mathbf{k}}^{\mathrm{hop}} + H_{-\mathbf{k}}^{\mathrm{hop}*}\right)\cos^2\frac{\theta}{2} \end{bmatrix} \boldsymbol{\beta}_{-\mathbf{k}}^\dagger + \mathrm{H.c.} \tag{C8b}$$

Importantly, if and only if the system has TRS, i.e., when Eq. (B22) holds, two local excitation modes become *decoupled*. In other words, three matrices defined in Eq. (B24) all become diagonal,

$$F = q \begin{bmatrix} \cos^2\bar{\theta} & 0 \\ 0 & \cos^2\frac{\theta}{2} \end{bmatrix}, \tag{C9a}$$

$$G = q \begin{bmatrix} \cos^2\theta & 0 \\ 0 & -\cos^2\frac{\theta}{2} \end{bmatrix}, \tag{C9b}$$

$$\mathcal{E} = \begin{bmatrix} 2z\tilde{t}\,\sin^2\bar{\theta} + \frac{1}{2}U\,\cos\bar{\theta} & 0 \\ 0 & z\tilde{t}\,\sin^2\bar{\theta} + \frac{1}{2}U\,\cos^2\frac{\bar{\theta}}{2} \end{bmatrix}. \tag{C9c}$$

Thus, the second-order term, Eq. (B15), can be written as

$$\hat{H}^{(2)} = \frac{1}{2} \sum_{\mathbf{k}} [\boldsymbol{\beta}_{\mathbf{k},A}^\dagger \quad \boldsymbol{\beta}_{-\mathbf{k},A} \quad \boldsymbol{\beta}_{\mathbf{k},P}^\dagger \quad \boldsymbol{\beta}_{-\mathbf{k},P}] \begin{bmatrix} H_{\mathbf{k},A}^{\mathrm{BdG}} & \\ & H_{\mathbf{k},P}^{\mathrm{BdG}} \end{bmatrix} \begin{bmatrix} \boldsymbol{\beta}_{\mathbf{k},A} \\ \boldsymbol{\beta}_{-\mathbf{k},A}^\dagger \\ \boldsymbol{\beta}_{\mathbf{k},P} \\ \boldsymbol{\beta}_{-\mathbf{k},P}^\dagger \end{bmatrix}, \tag{C10}$$

where

$$H_{\mathbf{k},\alpha}^{\mathrm{BdG}} = \begin{bmatrix} \xi_\alpha + \kappa_\alpha H_{\mathbf{k}}^{\mathrm{hop}} & \zeta_\alpha\kappa_\alpha H_{\mathbf{k}}^{\mathrm{hop}} \\ \zeta_\alpha\kappa_\alpha H_{\mathbf{k}}^{\mathrm{hop}} & \xi_\alpha + \kappa_\alpha H_{\mathbf{k}}^{\mathrm{hop}} \end{bmatrix} = \xi_\alpha\tau_0 \otimes I_{n_s} + \kappa_\alpha\tau_0 \otimes H_{\mathbf{k}}^{\mathrm{hop}} + \zeta_\alpha\kappa_\alpha\tau_1 \otimes H_{\mathbf{k}}^{\mathrm{hop}}, \tag{C11}$$

with all parameters given in Table I of the main text. Note we have renamed the local excitation modes $\alpha = 1 \to A$ and $\alpha = 2 \to P$, which represents the amplitude modes and phase modes, respectively. This nomenclature will be justified in the next Appendix.

A remarkable property of Eq. (C11) is that one can construct its Bogoliubov transformation analytically [76]. One first performs a unitary rotation using $\tilde{Q}_{\mathbf{k}} = \tau_0 \otimes Q_{\mathbf{k}}$, where $Q_{\mathbf{k}}$ diagonalizes the Bloch Hamiltonian $H_{\mathbf{k}}^{\mathrm{hop}}$, $Q_{\mathbf{k}}^\dagger H_{\mathbf{k}}^{\mathrm{hop}} Q_{\mathbf{k}} = D_{\mathbf{k}}$ with $D_{\mathbf{k}} = \mathrm{diag}(d_1, \ldots, d_{n_s})$. It then leads to

$$\tilde{Q}_{\mathbf{k}}^\dagger H_{\mathbf{k},\alpha}^{\mathrm{BdG}} \tilde{Q}_{\mathbf{k}} = \xi_\alpha\tau_0 \otimes I_{n_s} + \eta_\alpha\tau_0 \otimes D_{\mathbf{k}} + \zeta_\alpha\eta_\alpha\tau_1 \otimes D_{\mathbf{k}}. \tag{C12}$$

One then performs another pseudounitary transformation using

$$P_{\mathbf{k},\alpha} = \tau_0 \otimes \begin{bmatrix} \cosh\beta_{1,\mathbf{k},\alpha} & & \\ & \ddots & \\ & & \cosh\beta_{n_s,\mathbf{k},\alpha} \end{bmatrix} + \tau_1 \otimes \begin{bmatrix} \sinh\beta_{1,\mathbf{k},\alpha} & & \\ & \ddots & \\ & & \sinh\beta_{n_s,\mathbf{k},\alpha} \end{bmatrix}, \tag{C13}$$

where $\cosh\beta_{i,\mathbf{k},\alpha} = \sqrt{\frac{\xi_\alpha + d_{i,\mathbf{k}}}{2E_{i,\mathbf{k},\alpha}} + \frac{1}{2}}$, $\sinh\beta_{i,\mathbf{k},\alpha} = -\,\mathrm{sgn}(d_{i,\mathbf{k}})\sqrt{\frac{\xi_\alpha + d_{i,\mathbf{k}}}{2E_{i,\mathbf{k},\alpha}} - \frac{1}{2}}$ and

$$E_{i,\mathbf{k},\alpha}(d_{i\mathbf{k}}) = \sqrt{\xi_\alpha^2 + 2\xi_\alpha d_{i,\mathbf{k}}}. \tag{C14}$$

It then fully diagonalizes Eq. (C12),

$$P^{\dagger}_{\mathbf{k},\alpha}\tilde{Q}^{\dagger}_{\mathbf{k}}H^{\mathrm{BdG}}_{\mathbf{k},\alpha}\tilde{Q}_{\mathbf{k}}P_{\mathbf{k},\alpha} = \tau_0 \otimes \begin{bmatrix} E_{1,\mathbf{k},\alpha} & & & \\ & E_{2,\mathbf{k},\alpha} & & \\ & & \ddots & \\ & & & E_{n_s,\mathbf{k},\alpha} \end{bmatrix}. \tag{C15}$$

Thus, the pseudounitary matrix generally defined in Eq. (C2) now becomes

$$W_{\mathbf{k},\alpha} = \tilde{Q}_{\mathbf{k}}P_{\mathbf{k},\alpha}, \tag{C16}$$

or, more explicitly,

$$U_{\mathbf{k},\alpha} = Q_{\mathbf{k}}C_{\mathbf{k},\alpha}, \tag{C17a}$$

$$V_{\mathbf{k},\alpha} = Q_{\mathbf{k}}S_{\mathbf{k},\alpha}, \tag{C17b}$$

where

$$C_{\mathbf{k}} = \begin{bmatrix} \cosh\,\beta_{1,\mathbf{k},\alpha} & & \\ & \ddots & \\ & & \cosh\,\beta_{n_s,\mathbf{k},\alpha} \end{bmatrix}, \tag{C18a}$$

$$S_{\mathbf{k}} = \begin{bmatrix} \sinh\,\beta_{1,\mathbf{k},\alpha} & & \\ & \ddots & \\ & & \sinh\,\beta_{n_s,\mathbf{k},\alpha} \end{bmatrix}. \tag{C18b}$$

APPENDIX D: PHASE-AMPLITUDE CHARACTER

Here we discuss how to determine the phase-amplitude character of these excitation modes. Particularly, we show explicitly that the large filling limit of SSH-BHM has two types of excitations with pure phase and pure amplitude character, respectively. We only consider the momentum space version, the real-space version can be formulated similarly.

Consider the oscillation of the order parameter induced by a small perturbation above the ground state. For a perturbation characterized by an excitation labeled by momentum $\mathbf{k}$ and band index λ, the perturbed state evolves in time as $|\Psi_{\mathbf{k},\lambda}(t)\rangle = e^{-i\hat{H}t}(|G\rangle + \epsilon\gamma^{\dagger}_{\mathbf{k}\lambda}|G\rangle)$ with $\epsilon \ll 1$. Thus, the oscillation of the order parameter around the ground-state expectation value $\delta\phi_i(t) = \langle\Psi_{\mathbf{k},\lambda}(t)|\hat{a}_i|\Psi_{\mathbf{k},\lambda}(t)\rangle - \langle G|\hat{a}_i|G\rangle$ to linear order in ϵ, reads

$$\delta\phi_i(t) \propto \langle G|\hat{a}_i e^{-i\hat{H}^{(2)}t}\hat{\gamma}^{\dagger}_{\mathbf{k}\lambda}|G\rangle + \langle G|\hat{\gamma}_{\mathbf{k}\lambda}e^{i\hat{H}^{(2)}t}\hat{a}_i|G\rangle \tag{D1}$$

$$= \langle G|\hat{a}_i\hat{\gamma}^{\dagger}_{\mathbf{k}\lambda}|G\rangle e^{-i\omega_{\mathbf{k}\lambda}t} + \langle G|\hat{\gamma}_{\mathbf{k}\lambda}\hat{a}_i|G\rangle e^{i\omega_{\mathbf{k}\lambda}t} \tag{D2}$$

$$= \sum_{\alpha}[\mathcal{A}_{\alpha 0}(\langle G|\hat{\beta}^{\dagger}_{i\alpha}\hat{\gamma}^{\dagger}_{\mathbf{k}\lambda}|G\rangle e^{-i\omega_{\mathbf{k}\lambda}t} + \langle G|\hat{\gamma}_{\mathbf{k}\lambda}\hat{\beta}^{\dagger}_{i\alpha}|G\rangle e^{i\omega_{\mathbf{k}\lambda}t}) + \mathcal{A}_{0\alpha}(\langle G|\hat{\beta}_{i\alpha}\hat{\gamma}^{\dagger}_{\mathbf{k}\lambda}|G\rangle e^{-i\omega_{\mathbf{k}\lambda}t} + \langle G|\hat{\gamma}_{\mathbf{k}\lambda}\hat{\beta}_{i\alpha}|G\rangle e^{i\omega_{\mathbf{k}\lambda}t})] \tag{D3}$$

$$= \sum_{\mathbf{p},\alpha}\{\mathcal{A}_{\alpha 0}[\langle G|\hat{\beta}^{\dagger}_{\mathbf{p}\alpha\eta}\hat{\gamma}^{\dagger}_{\mathbf{k}\lambda}|G\rangle e^{-i(\omega_{\mathbf{k}\lambda}t+\mathbf{p}\cdot\mathbf{r}_i)} + \langle G|\hat{\gamma}_{\mathbf{k}\lambda}\hat{\beta}^{\dagger}_{\mathbf{p}\alpha\eta}|G\rangle e^{i(\omega_{\mathbf{k}\lambda}t-\mathbf{p}\cdot\mathbf{r}_i)}] + \mathcal{A}_{0\alpha}[\langle G|\hat{\beta}_{\mathbf{p}\alpha\eta}\hat{\gamma}^{\dagger}_{\mathbf{k}\lambda}|G\rangle e^{-i(\omega_{\mathbf{k}\lambda}t-\mathbf{p}\cdot\mathbf{r}_i)}$$

$$+ \langle G|\hat{\gamma}_{\mathbf{k}\lambda}\hat{\beta}_{\mathbf{p}\alpha\eta}|G\rangle e^{i(\omega_{\mathbf{k}\lambda}t+\mathbf{p}\cdot\mathbf{r}_i)}]\}. \tag{D4}$$

Using Eq. (C4) and the fact that $\gamma_{\mathbf{k}\lambda}|G\rangle = 0$, one has

$$\delta\phi_i(t) \propto X_{\mathbf{k}}e^{-i(\omega_{\mathbf{k}\lambda}t-\mathbf{k}\cdot\mathbf{r}_i)} + Y_{\mathbf{k}}e^{i(\omega_{\mathbf{k}\lambda}t-\mathbf{k}\cdot\mathbf{r}_i)}, \tag{D5}$$

where

$$X_{\mathbf{k}} = \sum_{\alpha}[\mathcal{A}_{\alpha 0}(V_{\mathbf{k}})_{\alpha\eta,\lambda} + \mathcal{A}_{0\alpha}(U_{\mathbf{k}})_{\alpha\eta,\lambda}], \tag{D6a}$$

$$Y_{\mathbf{k}} = \sum_{\alpha}[\mathcal{A}_{\alpha 0}(U^{*}_{\mathbf{k}})_{\alpha\eta,\lambda} + \mathcal{A}_{0\alpha}(V^{*}_{\mathbf{k}})_{\alpha\eta,\lambda}]. \tag{D6b}$$

Here the row of matrices U and V is labeled by two indices, the local excitation α and sublattice η. Thus, the imaginary (real) part of the order parameter oscillation is

$$\mathrm{Re}\ \delta\phi \propto X_{\mathbf{k}} + Y_{\mathbf{k}}, \tag{D7a}$$

$$\mathrm{Im}\ \delta\phi \propto X_{\mathbf{k}} - Y_{\mathbf{k}}. \tag{D7b}$$

A pure amplitude (phase) oscillation of the order parameter corresponds to Im $\delta\phi = 0$ (Re $\delta\phi = 0$), we define a flatness parameter,

$$F = \frac{|\text{Re } \delta\phi| - |\text{Im } \delta\phi|}{|\text{Re } \delta\phi| + |\text{Im } \delta\phi|} \in [-1, 1], \tag{D8}$$

to quantify the amplitude and phase components of an excitation: A positive (negative) flatness indicates dominant amplitude (phase) character. A pure amplitude (phase) oscillation corresponds to $F = 1$ (-1).

In the large filling limit, the flatness defined in Eq. (D8) can be obtained analytically. Using Eqs. (C7) and (C17), Eq. (D6) becomes for the $\alpha = A$ mode,

$$X_{\mathbf{k},A} = (Q_{\eta\lambda} \sinh \beta_{\lambda,\mathbf{k},A} + Q_{\eta\lambda} \cosh \beta_{\lambda,\mathbf{k},A}) \cos \bar{\theta}, \tag{D9a}$$

$$Y_{\mathbf{k},A} = (Q_{\eta\lambda} \cosh \beta_{\lambda,\mathbf{k},A} + Q_{\eta\lambda} \sinh \beta_{\lambda,\mathbf{k},A}) \cos \bar{\theta}, \tag{D9b}$$

hence, their difference vanishes. And for the $\alpha = P$ mode,

$$X_{\mathbf{k},P} = (\sinh \beta_{\lambda,\mathbf{k},P} Q_{\eta\lambda} - \cosh \beta_{\lambda,\mathbf{k},P} Q_{\eta\lambda}) \cos \frac{\bar{\theta}}{2}, \tag{D10a}$$

$$Y_{\mathbf{k},P} = (\cosh \beta_{\lambda,\mathbf{k},P} Q_{\eta\lambda} - \sinh \beta_{\lambda,\mathbf{k},P} Q_{\eta\lambda}) \cos \frac{\bar{\theta}}{2}, \tag{D10b}$$

hence, their sum vanishes. Here we have fixed the gauge by requiring $Q_{\eta\lambda}$ to be real. It then follows from Eq. (D7) that for the A mode $\delta\phi$ is purely real, whereas for the P mode $\delta\phi$ is purely imaginary, and the flatness is $+1$ and -1 for the A mode and the P mode, respectively, which justifies the nomenclature.

APPENDIX E: TOPOLOGICAL CHARACTER

In this Appendix, we discuss how to define the band topology for the bosonic BdG system of the 2D SSH-BHM. In particular, we prove that the topological index, namely, the symplectic polarization vector, is quantized to a $\mathbb{Z}_2$ number due to the inversion symmetry. And relate it to the parity eigenvalues at the inversion symmetric momenta. Then we show explicitly that in the infinite filling limit, the amplitude and phase bands have the same topological index as the underlying noninteracting Hamiltonian.

For a bosonic BdG system with the inversion symmetry defined by

$$\mathcal{I}_\tau H_{\mathbf{k}}^{\text{BdG}} \mathcal{I}_\tau^{-1} = H_{-\mathbf{k}}^{\text{BdG}}, \tag{E1}$$

the symplectic polarization defined in one dimension by Engelhardt and Brandes [18] can be straightforwardly generalized to the vectorized version,

$$\mathbf{P} = \frac{1}{(2\pi)^2} \int_{\text{BZ}} d^2k \, \mathbf{A}(\mathbf{k}), \tag{E2}$$

where the symplectic U(1) Berry connection is $A_\mu(\mathbf{k}) = i \sum_{\lambda_1 \leqslant \lambda \leqslant \lambda_2} \text{Tr}(\Gamma_\lambda W_{\mathbf{k}}^{-1} \partial_\mu W_{\mathbf{k}})$. We define a sewing matrix $B_{\mathbf{k}} = W_{-\mathbf{k}}^\dagger \Sigma_3 \mathcal{I}_\tau W_{\mathbf{k}}$ with $\Sigma_3 = \tau_3 \otimes I$ being the Pauli spin-z matrix acting on the Nambu space to relate eigenstates at momenta $\mathbf{k}$ and its inversion symmetric partner at $-\mathbf{k}$. Note this sewing matrix is pseudounitary, block diagonal, and satisfies $B_{-\mathbf{k}}^\dagger = B_{\mathbf{k}}$. Due to the inversion symmetry, we can relate the symplectic Berry connection at $\mathbf{k}$ to $-\mathbf{k}$ by using this sewing matrix,

$$A_\mu(-\mathbf{k}) = -A_\mu(\mathbf{k}) + i\partial_\mu \ln \det B_{\mathbf{k}}^<, \tag{E3}$$

where $B_{\mathbf{k}}^<$ denotes the projection of $B_{\mathbf{k}}$ to the block consisting of bands between $\lambda_1 \leqslant \lambda \leqslant \lambda_2$. Then for $\mu = 1$ (and similarly for $\mu = 2$), we have

$$\begin{aligned} P_1 &= \frac{1}{(2\pi)^2} \int_{-\pi}^{\pi} dk_2 \int_0^{\pi} dk_1 [A_1(k_1, k_2) + A_1(-k_1, k_2)] \\ &= \frac{1}{(2\pi)^2} \int_{-\pi}^{\pi} dk_2 \int_0^{\pi} dk_1 [A_1(k_1, k_2) - A_1(k_1, -k_2) \\ &\quad + i\partial_{k_1} \ln \det B_{\mathbf{k}}^<] \\ &= \frac{1}{2\pi} \int_{-\pi}^{\pi} dk_2 \left[\frac{i}{2\pi} \int_0^{\pi} dk_1 \partial_{k_1} \ln(\det B_{\mathbf{k}}^<) \right]. \end{aligned} \tag{E4}$$

Note the integral over k_1 gives the winding number of det $B_{\mathbf{k}}^<$, a pure phase at a fixed k_2. Since the system under consideration has TRS, namely, the Chern number always vanishes, which means that one can always find a continuous gauge. Thus, the winding number cannot change discontinuously along the k_2 direction, and we can simply evaluate this constant by taking $k_2 = 0$, which leads to

$$P_1 = \frac{i}{2\pi} \int_0^{\pi} dk_1 \partial_{k_1} \ln \det B_{k_1,0}^< = \frac{i}{2\pi} \ln \frac{\det B_{\mathbf{X}_1}^<}{\det B_{\mathbf{\Gamma}}^<}. \tag{E5}$$

Since at the inversion symmetric momenta, we have $\Sigma_3 B_{\mathbf{k}_{\text{inv}}} = \Sigma_3 W_{\mathbf{k}_{\text{inv}}}^\dagger \Sigma_3 \mathcal{I}_\tau W_{\mathbf{k}_{\text{inv}}} = W_{\mathbf{k}_{\text{inv}}}^{-1} \mathcal{I}_\tau W_{\mathbf{k}_{\text{inv}}}$, which leads to det $B_{\mathbf{k}_{\text{inv}}}^< = \pm \prod_{\lambda_1 \leqslant \lambda \leqslant \lambda_2} \eta_{\mathbf{k}_{\text{inv}}}$ (plus or minus sign for particle or hole space), where η is the eigenvalue of the inversion operator $\mathcal{I}_\tau$. In conclusion, each component of $\mathbf{P}$ is quantized to a $\mathbb{Z}_2$ number,

$$P_\mu = \frac{1}{2} \left(\sum_{\lambda_1 \leqslant \lambda \leqslant \lambda_2} n_{\lambda,\mu} \mod 2 \right), \tag{E6}$$

where $(-1)^{n_{\lambda,\mu}} = \eta_\lambda(X_\mu)\eta_\lambda(\Gamma)$.

At the infinite filling limit since two modes are decoupled, we can study Eq. (C11) for $\alpha = A, P$, individually. This BdG Hamiltonian is easily seen to satisfy the inversion symmetry Eq. (E1) with

$$\mathcal{I}_\tau = \tau_0 \otimes \mathcal{I}. \tag{E7}$$

Since $E_{i,\mathbf{k},\alpha}(d_{i\mathbf{k}})$ defined in Eq. (C14) is a monotonically increasing function, the band gap closes at the same t_1/t_2 and at the same $\mathbf{k}$ points in the BZ for the noninteracting bands $d_{i\mathbf{k}}$ and the BdG bands $E_{i,\mathbf{k},\alpha}$. Moreover, the parity eigenvalues for these two systems are also the same,

$$\begin{aligned} W_{\mathbf{k}}^{-1} \mathcal{I}_\tau W_{\mathbf{k}} &= \Sigma_3 W_{\mathbf{k}}^\dagger \Sigma_3 (\tau_0 \otimes \mathcal{I}) W_{\mathbf{k}} \\ &= \Sigma_3 P_{\mathbf{k}}^\dagger \tilde{Q}_{\mathbf{k}}^\dagger \Sigma_3 (\tau_0 \otimes \mathcal{I}) \tilde{Q}_{\mathbf{k}} P_{\mathbf{k}} \\ &= \Sigma_3 P_{\mathbf{k}}^\dagger [\tau_3 \otimes (Q_{\mathbf{k}}^{-1} \mathcal{I} Q_{\mathbf{k}})] P_{\mathbf{k}} \\ &= \tau_0 \otimes (Q_{\mathbf{k}}^{-1} \mathcal{I} Q_{\mathbf{k}}), \end{aligned} \tag{E8}$$

where to arrive at the last line, we have used the explicit form of matrix $P_{\mathbf{k}}$ given in Eq. (C13). We, thus, conclude that the topological phase boundary does not alter.

In the finite filling case, our bosonic BdG Hamiltonian still obeys the inversion symmetry $\tilde{I} = I_4 \otimes \mathcal{I}$. We

numerically find that the topological transition point again occurs at $t_1 = t_2$, which is understandable from the symmetric roles played by two hopping parameters.

APPENDIX F: A GINZBURG-LANDAU ANALYSIS VIA STRONG-COUPLING RANDOM-PHASE APPROXIMATION

Here we derive the effective action used in the main text, following a strong-coupling random-phase approximation developed by Sengupta and Dupuis [68] and discuss the condition leads to the (approximate) particle-hole symmetry.

In the imaginary-time path-integral formalism, the Euclidean action is

$$S = \int_0^\beta d\tau \Big[\sum_i a_i^* \partial_\tau a_i - \sum_{ij} t_{ij} a_i^* a_j - \mu \sum_i a_i^* a_i + \frac{1}{2} U \sum_i |a_i|^4 \Big]. \tag{F1}$$

Using a Hubbard-Stratonovich (HS) transformation, we introduce an auxiliary field φ to decouple the hopping term and integrate out the original field a, the partition function formally becomes

$$Z = Z_0 \int \mathcal{D}[\varphi^*, \varphi] \exp\Big\{ - \int_0^\beta d\tau \sum_i \varphi_i^*(\tau)(t^{-1})_{ij}\varphi_j(\tau) + W_{\rm loc}[\varphi^*, \varphi] \Big\}. \tag{F2}$$

The generating functional for connected l-particle local Green's function is defined by

$$\begin{aligned} G_{\rm loc}^{c,(l)}(\tau_1, \ldots, \tau_l; \tau_1', \ldots, \tau_l') &= (-1)^l \langle a_i(\tau_1) \cdots a_i(\tau_l) a_i^*(\tau_l') \cdots a_i^*(\tau_1') \rangle_{\rm loc} \\ &= (-1)^l \frac{\delta^{(2l)} W_{\rm loc}[\varphi^*, \varphi]}{\delta\varphi_i^*(\tau_1) \cdots \delta\varphi_i^*(\tau_l) \delta\varphi_i(\tau_l') \cdots \delta\varphi_i(\tau_1')}. \end{aligned} \tag{F3}$$

Here the local Hamiltonian is

$$\hat{H}_{\rm loc} = \sum_i \Big[\frac{1}{2} U \hat{n}_i(\hat{n}_i - 1) - \mu \hat{n}_i \Big], \tag{F4}$$

and $\langle \cdots \rangle_{\rm loc}$ means that the average is taken with respect to $\hat{H}_{\rm loc}$. Upon reverting the above equation, we obtain

$$W_{\rm loc}[\varphi^*, \varphi] = \sum_{l=1}^\infty \frac{(-1)^l}{(l!)^2} \int d\tau_1 \cdots d\tau_l G_{\rm loc}^{c,(l)}(\tau_1, \ldots, \tau_l; \tau_1', \ldots, \tau_l') \varphi^*(\tau_1) \cdots \varphi^*(\tau_l) \varphi(\tau_l') \cdots \varphi(\tau_1'). \tag{F5}$$

The effective action given in Eq. (F2) is used by Refs. [45,77] to study the quantum phase transition between the SF phase and the MI phase. However, as pointed out by Sengupta and Dupuis [68] in the SF phase, the Green's function obtained is not physical, thus, the excitation spectrum is out of reach. More importantly, it is hard to investigate the topology associated with the inverse of the hopping matrix, being generally a complicated infinite-range hopping matrix.

We can kill two birds with one stone by performing a second HS transformation. This process decouples the hopping term in Eq. (F2) where the pure local φ field can be integrated out again. Since the correlation function built from the auxiliary field introduced in this second HS transformation and the original bosonic fields a are the same (the proof is easy and can be found in Ref. [68]), we use the same notation for them. The resulting effective action is

$$\begin{aligned} S^{\rm eff} = &\int d\tau\, d\tau' \sum_{ij} \big\{ a_i^*(\tau) \big[-\Gamma_{\rm loc}^{(1)}(\tau;\tau')\delta_{ij} + t_{ij}\delta(\tau - \tau') \big] a_j(\tau') \big\} \\ &+ \int d\tau_1 d\tau_2 d\tau_1' d\tau_2' \sum_i \Big[\frac{1}{4} \Gamma_{\rm loc}^{(2)}(\tau_1, \tau_2; \tau_2', \tau_1') a_i^*(\tau_1) a^*(\tau_2) a_i(\tau_2') a_i(\tau_1') \Big] + \cdots, \end{aligned} \tag{F6}$$

where $\cdots$ denotes higher-order local vertex functions, which are neglected. Here, the one-particle local vertex function is given by $\Gamma_{\rm loc}^{(1)} = [G_{\rm loc}^{(1)}]^{-1}$ (from here on we will omit the superscript in $G^{(1)}$ for the single-particle Green's function). And the two-particle local vertex function $\Gamma_{\rm loc}^{(2)}$ can be obtained from the one- and two-particle connected local Green's function using the standard formula [78],

$$G_{\rm loc}^{c,(2)}(\tau_1, \tau_2; \tau_1', \tau_2') = -\int_0^\beta d\tau_3 d\tau_4 d\tau_3' d\tau_4' G_{\rm loc}(\tau_1;\tau_3) G_{\rm loc}(\tau_2;\tau_4) \Gamma_{\rm loc}^{(2)}(\tau_3, \tau_4; \tau_3', \tau_4') G_{\rm loc}(\tau_3';\tau_1') G_{\rm loc}(\tau_4';\tau_2'). \tag{F7}$$

Before proceeding further, we review the local problem defined by Eq. (F4). For a given site, it is already diagonal in particle number basis. The ground state has q bosons with $q = \lfloor \mu/U \rfloor + 1$ if $\mu > 0$, and $q = 0$ otherwise, and the corresponding energy $e_q = -\mu q + (U/2)q(q-1)$. The single-particle Green's function is (for $\tau > 0$)

$$G_{\rm loc}(\tau; 0) = -\langle T_\tau a(\tau) a^\dagger(0) \rangle = -\frac{1}{Z_{\rm loc}} \sum_{n=0}^\infty (n+1) e^{-(\beta-\tau)e_n - \tau e_{n+1}}, \tag{F8}$$

where $Z_{\rm loc} = \sum_{n=0}^{\infty} e^{-\beta e_n}$. In Matsubara frequency space at zero temperature, it becomes

$$G_{\rm loc}(i\omega)|_{T=0} = \lim_{\beta\to\infty} \int_0^\beta d\tau\, G_{\rm loc}(\tau;0) e^{i\omega\tau} = \frac{-q}{i\omega + e_{q-1} - e_q} + \frac{q+1}{i\omega + e_q - e_{q+1}}. \tag{F9}$$

The two-particle Green's function can be obtained similarly, whose explicit expression in the static limit at zero temperature $\bar{G}^{c,(2)}_{\rm loc}$ can be found in Ref. [68]. If we approximate $\Gamma^{(2)}_{\rm loc}$ by its static value $\bar{\Gamma}^{(2)}_{\rm loc} = -\bar{G}^{c,(2)}_{\rm loc}/\bar{G}^4_{\rm loc}$ and introducing $\tilde{U} = \frac{1}{2}\bar{\Gamma}^{(2)}_{\rm loc}$, the effective action then reads

$$S^{\rm eff} = \int d\tau\, d\tau' \sum_{ij} a_i^*(\tau)\big[-G^{-1}_{\rm loc}(\tau;\tau')\delta_{ij} + t_{ij}\delta(\tau-\tau')\big]a_j(\tau') + \frac{1}{2}\tilde{U}\int d\tau \sum_i |a_i(\tau)|^4. \tag{F10}$$

In Matsubara frequency space, using Eq. (F9), one can expand $G^{-1}_{\rm loc}(i\omega)$ around $\omega = 0$,

$$-G^{-1}_{\rm loc}(i\omega) = \frac{(-qU+\mu+i\omega)(U-qU+\mu+i\omega)}{U+\mu+i\omega} = \sum_{\ell=0}^{\infty} c_\ell (i\omega)^\ell, \tag{F11}$$

where $c_\ell = (\ell!)^{-1}\partial^l G^{-1}_{\rm loc}(i\omega)/\partial(i\omega)^l|_{\omega=0}$, and the most important coefficient is

$$c_1 = -1 + \frac{q(1+q)U^2}{(U+\mu)^2}, \tag{F12}$$

whose vanishing on the μ-t phase diagram is the so-called PH symmetric line $\mu_{\rm phs} = [\sqrt{q(1+q)} - 1]U$. Note it starts at the tip of the qth lobe and is a horizontal line independent of zt, which overlooks the hopping effects in comparison with Eq. (B7). Precisely at the PH symmetric line, Eq. (F11) becomes

$$-G^{-1}_{\rm loc}(i\omega)|_{\mu=\mu_{\rm phs}} = \frac{[-1+i\omega-q+\sqrt{q(1+q)}][i\omega-q+\sqrt{q(1+q)}]}{i\omega+\sqrt{q(1+q)}}, \tag{F13}$$

which leads to

$$c_\ell|_{\mu=\mu_{\rm phs}} = \left[\frac{-1}{\sqrt{q(1+q)}}\right]^{\ell-1} = O(q^{-\ell+1}), \quad \text{for } \ell > 1. \tag{F14}$$

Thus, at the large filling limit and on the PH symmetric line, only c_2 survives even away from the low-energy limit.

APPENDIX G: A BRIEF DISCUSSION ON THE VALIDITY OF THE SLAVE BOSON METHOD

Generally speaking as a strong-coupling expansion, our approach is expected to work well in the Mott-insulating phase and in the superfluid phase close to the SF-MI phase transition boundary; and to become worse in the weakly interacting limit (where the standard Bogoliubov theory should be more appropriate).

More specifically, we note that the local Hilbert space is enlarged when the slave bosons are introduced at each site; however, this redundancy is then removed by imposing the local constraint. There are two main approximations involved: (1) Only three local states at each sites are considered. (2) The local constraint is actually broken when condensing β_G and making the replacement Eq. (B14) with higher-order terms omitted.

Regarding the first issue, we note that, in the vicinity of the Mott phase, number fluctuations are small, which allows one to truncate the Hilbert space into the subspace of the lowest local number states. This local number fluctuations have also been experimentally measured [46] and found, indeed, to be suppressed due to strong interactions near the vicinity of the Mott phase. Moreover, this approximation can be systematically improved by the inclusion of further local states. The error occurred by this truncation can be computed by comparing the two cases. We have numerically checked that such an error is, indeed, small for parameter regions of our interests. In fact, by including these extra local states, we find that the resulting spurious excitations are almost equal two-,three-,...particle excitations of the mean-field Hamiltonian Eq. (A1), reflecting the fact that they are high-energy excitations, outside of our low-energy theory in the strong-coupling limit.

Regarding the second issue, the same approximation also occurs in the widely used method of the Holstein-Primakoff boson [79] and the standard Bogoliubov theory [80]. One way to verify the validity of this approximation is to check that *a posteriori* the quantum depletion $\sum_{\alpha\neq G}\langle\beta^\dagger_{i,\alpha}\beta_{i,\alpha}\rangle$ is, indeed, quite small comparing to unit. A similar calculation has been performed in Ref. [48] (for the standard Bose-Hubbard model in 2D): this quantity is around 0.2 and is largest at the phase-transition point. Therefore, the expansion Eq. (B14) is justified, and it should be a good approximation for the parameter region of our interests. Interaction among the Higgs and the Goldstone modes can be studied in the future by including these higher-order terms in the expansion Eq. (B14).

[1] K. v. Klitzing, G. Dorda, and M. Pepper, Phys. Rev. Lett. **45**, 494 (1980).
[2] D. J. Thouless, M. Kohmoto, M. P. Nightingale, and M. den Nijs, Phys. Rev. Lett. **49**, 405 (1982).
[3] F. D. M. Haldane and S. Raghu, Phys. Rev. Lett. **100**, 013904 (2008).
[4] L. Lu, J. D. Joannopoulos, and M. Soljačić, Nat. Photonics **8**, 821 (2014).
[5] T. Ozawa, H. M. Price, A. Amo, N. Goldman, M. Hafezi, L. Lu, M. C. Rechtsman, D. Schuster, J. Simon, O. Zilberberg, and I. Carusotto, Rev. Mod. Phys. **91**, 015006 (2019).
[6] R. Suesstrunk and S. D. Huber, Science **349**, 47 (2015).
[7] Y. Liu, X. Chen, and Y. Xu, Adv. Funct. Mater. **30**, 1904784 (2020).
[8] R. Shindou, R. Matsumoto, S. Murakami, and J.-i. Ohe, Phys. Rev. B **87**, 174427 (2013).
[9] D. G. Joshi and A. P. Schnyder, Phys. Rev. B **100**, 020407(R) (2019).
[10] H. Kondo, Y. Akagi, and H. Katsura, Prog. Theor. Exp. Phys. **2020**, 12A104 (2020).
[11] X. S. Wang and X. R. Wang, J. Appl. Phys. **129**, 151101 (2021).
[12] Z. Yang, F. Gao, X. Shi, X. Lin, Z. Gao, Y. Chong, and B. Zhang, Phys. Rev. Lett. **114**, 114301 (2015).
[13] S. D. Huber, Nat. Phys. **12**, 621 (2016).
[14] G. Ma, M. Xiao, and C. T. Chan, Nat. Rev. Phys. **1**, 281 (2019).
[15] P. Delplace, J. B. Marston, and A. Venaille, Science **358**, 1075 (2017).
[16] Z. Wu, L. Zhang, W. Sun, X.-T. Xu, B.-Z. Wang, S.-C. Ji, Y. Deng, S. Chen, X.-J. Liu, and J.-W. Pan, Science **354**, 83 (2016).
[17] Z.-Y. Wang, X.-C. Cheng, B.-Z. Wang, J.-Y. Zhang, Y.-H. Lu, C.-R. Yi, S. Niu, Y. Deng, X.-J. Liu, S. Chen *et al.*, Science **372**, 271 (2021).
[18] G. Engelhardt and T. Brandes, Phys. Rev. A **91**, 053621 (2015).
[19] S. Furukawa and M. Ueda, New J. Phys. **17**, 115014 (2015).
[20] M. Di Liberto, A. Hemmerich, and C. Morais Smith, Phys. Rev. Lett. **117**, 163001 (2016).
[21] J.-S. Pan, W. Zhang, W. Yi, and G.-C. Guo, Phys. Rev. A **94**, 043619 (2016).
[22] Z.-F. Xu, L. You, A. Hemmerich, and W. V. Liu, Phys. Rev. Lett. **117**, 085301 (2016).
[23] Y.-J. Wu, W.-Y. Zhou, and S.-P. Kou, Phys. Rev. A **95**, 023620 (2017).
[24] G.-Q. Luo, A. Hemmerich, and Z.-F. Xu, Phys. Rev. A **98**, 053617 (2018).
[25] T. Ohashi, S. Kobayashi, and Y. Kawaguchi, Phys. Rev. A **101**, 013625 (2020).
[26] J. Wang, W. Zheng, and Y. Deng, Phys. Rev. A **102**, 043323 (2020).
[27] G.-H. Huang, G.-Q. Luo, Z. Wu, and Z.-F. Xu, Phys. Rev. A **103**, 043328 (2021).
[28] L.-L. Wan, Z. Zhou, and Z.-F. Xu, Phys. Rev. A **103**, 013308 (2021).
[29] X.-Q. Wang, G.-Q. Luo, J.-Y. Liu, W. V. Liu, A. Hemmerich, and Z.-F. Xu, Nature (London) **596**, 227 (2021).
[30] Y. Nambu and G. Jona-Lasinio, Phys. Rev. **122**, 345 (1961).
[31] J. Goldstone, Il Nuovo Cimento **19**, 154 (1961).
[32] S. Weinberg, *The Quantum Theory of Fields* (Cambridge University Press, Cambridge, UK, 1995), Vol. 2.
[33] P. W. Higgs, Phys. Rev. Lett. **13**, 508 (1964).
[34] G. Aad, T. Abajyan, B. Abbott, J. Abdallah, S. A. Khalek, A. A. Abdelalim, R. Aben, B. Abi, M. Abolins, O. S. AbouZeid *et al.*, Phys. Lett. B **716**, 1 (2012).
[35] S. Chatrchyan, V. Khachatryan, A. M. Sirunyan, A. Tumasyan, W. Adam, E. Aguilo, T. Bergauer, M. Dragicevic, J. Erö, C. Fabjan *et al.*, Phys. Lett. B **716**, 30 (2012).
[36] D. Pekker and C. M. Varma, Annu. Rev. Condens. Matter Phys. **6**, 269 (2015).
[37] D. Sherman, U. S. Pracht, B. Gorshunov, S. Poran, J. Jesudasan, M. Chand, P. Raychaudhuri, M. Swanson, N. Trivedi, A. Auerbach *et al.*, Nat. Phys. **11**, 188 (2015).
[38] S. Tsuchiya, D. Yamamoto, R. Yoshii, and M. Nitta, Phys. Rev. B **98**, 094503 (2018).
[39] R. Shimano and N. Tsuji, Annu. Rev. Condens. Matter Phys. **11**, 103 (2020).
[40] R. Yusupov, T. Mertelj, V. V. Kabanov, S. Brazovskii, P. Kusar, J.-H. Chu, I. R. Fisher, and D. Mihailovic, Nat. Phys. **6**, 681 (2010).
[41] S.-M. Souliou, J. Chaloupka, G. Khaliullin, G. Ryu, A. Jain, B. J. Kim, M. Le Tacon, and B. Keimer, Phys. Rev. Lett. **119**, 067201 (2017).
[42] A. Jain, M. Krautloher, J. Porras, G. H. Ryu, D. P. Chen, D. L. Abernathy, J. T. Park, A. Ivanov, J. Chaloupka, G. Khaliullin *et al.*, Nat. Phys. **13**, 633 (2017).
[43] O. Avenel, E. Varoquaux, and H. Ebisawa, Phys. Rev. Lett. **45**, 1952 (1980).
[44] C. A. Collett, J. Pollanen, J. I. A. Li, W. J. Gannon, and W. P. Halperin, J. Low Temp. Phys. **171**, 214 (2013).
[45] M. P. A. Fisher, P. B. Weichman, G. Grinstein, and D. S. Fisher, Phys. Rev. B **40**, 546 (1989).
[46] M. Greiner, O. Mandel, T. Esslinger, T. W. Hänsch, and I. Bloch, Nature (London) **415**, 39 (2002).
[47] E. Altman and A. Auerbach, Phys. Rev. Lett. **89**, 250404 (2002).
[48] S. D. Huber, E. Altman, H. P. Büchler, and G. Blatter, Phys. Rev. B **75**, 085106 (2007).
[49] L. Pollet and N. Prokof'ev, Phys. Rev. Lett. **109**, 010401 (2012).
[50] L. Liu, K. Chen, Y. Deng, M. Endres, L. Pollet, and N. Prokof'ev, Phys. Rev. B **92**, 174521 (2015).
[51] M. Di Liberto, A. Recati, N. Trivedi, I. Carusotto, and C. Menotti, Phys. Rev. Lett. **120**, 073201 (2018).
[52] U. Bissbort, S. Götze, Y. Li, J. Heinze, J. S. Krauser, M. Weinberg, C. Becker, K. Sengstock, and W. Hofstetter, Phys. Rev. Lett. **106**, 205303 (2011).
[53] M. Endres, T. Fukuhara, D. Pekker, M. Cheneau, P. Schauβ, C. Gross, E. Demler, S. Kuhr, and I. Bloch, Nature (London) **487**, 454 (2012).
[54] W. P. Su, J. R. Schrieffer, and A. J. Heeger, Phys. Rev. Lett. **42**, 1698 (1979).
[55] W. A. Benalcazar, B. A. Bernevig, and T. L. Hughes, Phys. Rev. B **96**, 245115 (2017).
[56] W. A. Benalcazar, B. A. Bernevig, and T. L. Hughes, Science **357**, 61 (2017).
[57] F. Liu and K. Wakabayashi, Phys. Rev. Lett. **118**, 076803 (2017).
[58] R. Resta, Rev. Mod. Phys. **66**, 899 (1994).
[59] C. Fang, M. J. Gilbert, and B. A. Bernevig, Phys. Rev. B **86**, 115112 (2012).

[60] L. Fu and C. L. Kane, Phys. Rev. B **76**, 045302 (2007).
[61] R. Fresard, arXiv:cond-mat/9405053.
[62] E. Altman, W. Hofstetter, E. Demler, and M. D. Lukin, New J. Phys. **5**, 113 (2003).
[63] D. B. M. Dickerscheid, D. van Oosten, P. J. H. Denteneer, and H. T. C. Stoof, Phys. Rev. A **68**, 043623 (2003).
[64] D. Pekker, B. Wunsch, T. Kitagawa, E. Manousakis, A. S. Sørensen, and E. Demler, Phys. Rev. B **86**, 144527 (2012).
[65] D. Huerga, J. Dukelsky, and G. E. Scuseria, Phys. Rev. Lett. **111**, 045701 (2013).
[66] I. Frérot and T. Roscilde, Phys. Rev. Lett. **116**, 190401 (2016).
[67] Equivalently, one may parametrize the ground-state wave function as given in (B2), then minimize the corresponding ground-state energy. Details can be found in Appendix B.
[68] K. Sengupta and N. Dupuis, Phys. Rev. A **71**, 033629 (2005).
[69] V. Peano and H. Schulz-Baldes, J. Math. Phys. **59**, 031901 (2018).
[70] Y. Akagi, J. Phys. Soc. Jpn. **89**, 123601 (2020).
[71] X. S. Wang, A. Brataas, and R. E. Troncoso, Phys. Rev. Lett. **125**, 217202 (2020).
[72] A. L. Gaunt, T. F. Schmidutz, I. Gotlibovych, R. P. Smith, and Z. Hadzibabic, Phys. Rev. Lett. **110**, 200406 (2013).
[73] H. Katsura, N. Nagaosa, and P. A. Lee, Phys. Rev. Lett. **104**, 066403 (2010).
[74] D. van Oosten, P. van der Straten, and H. T. C. Stoof, Phys. Rev. A **63**, 053601 (2001).
[75] L. D. Landau and E. M. Lifshitz, *Quantum Mechanics: Non-Relativistic Theory* (Elsevier, Amsterdam, 2013), Vol. 3.
[76] P. S. Kumar, I. F. Herbut, and R. Ganesh, Phys. Rev. Res. **2**, 033035 (2020).
[77] S. Sachdev, *Quantum Phase Transitions* (Cambridge University Press, Cambridge, UK, 2011).
[78] J. W. Negele and H. Orland, *Quantum Many-Particle Systems* (CRC, Baton Rouge, FL, 2018).
[79] A. Auerbach, *Interacting Electrons and Quantum Magnetism* (Springer, Berlin, 2012).
[80] Y. Kawaguchi and M. Ueda, Phys. Rep. **520**, 253 (2012).